

铜 - 稀土单分子磁体的研究进展

郑祺¹, 张腾坤¹, 王窦尊¹, 徐航¹, 李嘉欣¹, 崔会会¹, 孙广平¹, 王金^{1,2,*}

¹南通大学化学化工学院, 江苏 南通

²南通智能与新能源材料重点实验室, 江苏 南通

收稿日期: 2024年6月19日; 录用日期: 2024年8月14日; 发布日期: 2024年8月28日

摘要

在3d-4f类型中的单分子磁体里, 铜通常以二价的形式存在, 并且它的特征电子构型为3d⁹, 因此被认为是顺磁中心。在八面体配位环境中, Cu^{II}的d层轨道分裂成了t_{2g}⁶e_g³, 这就导致了Cu^{II}中会出现Jahn-Teller效应。结合这些特性, Cu^{II}会表现出中等的磁各向异性, 因此通常被认为是各向同性离子。然而, 由于其灵活的配位性, 以及它会与4f金属形成强铁磁耦合的能力, Cu-Ln SMMs仍然是研究的焦点。

关键词

铜 - 稀土单分子磁体, 结构, 磁性

Research Progress in Cu-Ln SMMs Single Molecule Magnets

Qi Zheng¹, Tengkun Zhang¹, Douzun Wang¹, Hang Xu¹, Jiaxin Li¹, Huihui Cui¹, Guangping Sun¹, Jin Wang^{1,2*}

¹School of Chemistry and Chemical Engineering, Nantong University, Nantong Jiangsu

²Nantong Key Laboratory of Intelligent and New Energy Materials and Devices, Nantong Jiangsu

Received: Jun. 19th, 2024; accepted: Aug. 14th, 2024; published: Aug. 28th, 2024

Abstract

In 3d-4f SMMs, copper is typically present in the Cu^{II} form, characterized by 3d⁹ electron configuration, and is thus commonly regarded as paramagnetic center. In octahedral coordination environment, the d orbitals of Cu^{II} split into t_{2g}⁶e_g³, leading to the occurrence of the Jahn-Teller effect in Cu^{II}. Combining these characteristics, Cu^{II} exhibits moderate magnetic anisotropy, and thus is often

*通讯作者 Email: wangjin110@ntu.edu.cn

regarded as isotropic ion. However, due to its flexible coordination, along with its ability to form strong ferromagnetic couplings with 4f metals, Cu-Ln SMMs have remained the focal point of research.

Keywords

Cu-Ln Single Molecule Magnets, Structure, Magnetism

Copyright © 2024 by author(s) and Hans Publishers Inc.

This work is licensed under the Creative Commons Attribution International License (CC BY 4.0).

<http://creativecommons.org/licenses/by/4.0/>



Open Access

1. 引言

近年来，单分子磁体(Single-Molecule Magnets, SMMs)作为一种新兴的磁性材料，受到了广泛的关注[1]。单分子磁体是一类在低温下能够表现出磁双稳态的有机金属化合物，其独特的磁性质使其在信息存储[2]、量子计算[3]、磁制冷[4]等领域具有重要应用前景。在众多类型的单分子磁体中，过渡 - 稀土配合物因其独特的磁各向异性，成为研究的热点[5] [6]。

铜 - 稀土单分子磁体(Cu-Ln SMMs)是过渡金属 - 稀土配合物中的一个重要分支。铜离子 Cu^{2+} 具有较高的电子自旋态($S = 1/2$)，与稀土离子(如 Dy^{3+} 、 Tb^{3+})的强磁各向异性相结合，可以形成具有显著单分子磁性的配合物[7]。这类配合物在低温下能够表现出磁滞回线等典型的单分子磁体特性。近年来，随着合成技术和表征手段的进步，研究者们在铜 - 稀土单分子磁体的结构设计、磁性调控等方面取得了诸多重要进展(表 1)。铜 - 稀土单分子磁体的结构设计是实现其优异磁性的基础，通过合理设计配体、调控金属离子间的相互作用，能够有效的提高单分子磁体的阻磁能垒[8]-[10]。例如，研究发现，使用具有强配位能力的配体可以显著增强铜离子和稀土离子之间的超交换作用，从而提升单分子磁体的磁学性能[11]。其次，磁性调控是铜 - 稀土单分子磁体研究中的另一重要方面。通过更换配体、外加磁场等手段，可以对单分子磁体的磁性质进行有效调控[12] [13]。近年来有研究表明，通过对配体进行官能团修饰，可以改变配合物的晶体场环境，从而调节其磁各向异性和磁弛豫行为[4] [14]-[17]。

总之，铜 - 稀土单分子磁体作为一种具有巨大潜力的磁性材料，近年来在结构设计、磁性调控等方面取得了显著进展[18] [19]。本文通过对近年来典型的例子进行综述，以期为 3d-4f 单分子磁体的发展奠定一定的基础。

2. 铜 - 稀土单分子磁体的研究进展

目前，已报道的铜 - 稀土单分子磁体如表 1 所示，本论文仅选其中一些例子进行描述，并根据其核数进行排序，以研究其结构与磁性行为之间的关系。通过对比和分析，发现配体的选择和配位方式尤为关键，通过引入不同配体可以改变配合物的构型，电荷排列方式，进一步改变配合物的弛豫路径，从而获得不同的能垒。而核数也是至关重要的，随着 Cu-Ln SMMs 中核数的增加，磁相互作用的复杂性也随之增加，这给预测和模拟磁行为带来了挑战。例如，随着核数的增加，使之对于结构的精确设计从而保持所需的磁特性变得越发有难度，分子内金属与金属的磁相互作用的类型增加，使磁耦合路径分析复杂化，导致对体系表现出的磁性解释更具有挑战。但同时，增加核数也可以增强总的自旋基态，增强磁各向异性，提高分子的磁性能，通常会表现出较长的弛豫时间。还有一个优点，那就是核数的增加可能会

抑制量子隧穿，这也是因为多核的复杂磁相互作用增加能量势垒的原因之一。目前的研究进展就是通过不同的合成策略来调控配合物的磁性，例如，通过改变配体的种类或引入新的金属中心，优化磁各向异性和能垒大小，提高在高温区的稳定性和磁性能。

Table 1. The magnetic data of Cu-Ln SMMs
表 1. 铜 - 稀土单分子磁体的磁性数据

complexes	H_{dc}/kOe	U_{eff}/K	τ_0/s	$v/\text{mT/s}$	T_B/K	Ref.
[TbCu(L ¹)(NO ₃) ₃ (H ₂ O)] (1)	1	29(2)				[20]
[TbCu(L ¹)(o-vanilate)(NO ₃)(MeOH)]·NO ₃ (2)	1	32.2(6)				[20]
[Cu(L ²)(C ₃ H ₆ O)Tb(NO ₃) ₃] (3)	1	42.3(4)	$7.1(9) \times 10^{-10}$			[21]
[Cu(L ²)(C ₃ H ₆ O)Dy(NO ₃) ₃] (4)	1	11.5(10)	$4(2) \times 10^{-10}$			[21]
[{Dy(hfac) ₃ } ₂ {Cu(dpk) ₂ }] (5)	0	47(4)	$1.1(5) \times 10^{-7}$			[22]
[Cu ₂ (L ³) ₂ DyCl ₂ (H ₂ O)]·Cl·MeCN (6)	0	39.06	1.05×10^{-5}			[23]
[Cu(L ⁴)Tb(hfac) ₂] ₂ (7)	0	21	2.7×10^{-8}			[24]
[Cu ₂ (valpn) ₂ Tb ₂ (N ₃) ₆]·2CH ₃ OH (8)	0	30.1 ± 0.7	$1.1 \pm 0.2 \times 10^{-6}$	50	2.4	[25]
[Tb ₂ Cu ₃ (H ₃ L ⁵) ₂ (CH ₃ COO) ₆]·CH ₃ OH·2H ₂ O (10)	0	21.4 ± 0.5	1.3×10^{-7}			[26]
(NMe ₄) ₂ [Tb ₂ Cu ₃ (H ₃ L ⁵) ₂ (NO ₃) ₇ (CH ₃ OH) ₂]·(NO ₃) (11)	0	36.0 ± 0.2	1.0×10^{-7}	140	1.8	[26]
(NMe ₄) ₂ [Dy ₂ Cu ₃ (H ₃ L ⁵) ₂ (NO ₃) ₇ (CH ₃ OH) ₂]·(NO ₃) (12)	0	23.9 ± 0.1	7.5×10^{-8}			[26]
(NMe ₄) ₂ [Ho ₂ Cu ₃ (H ₃ L ⁵) ₂ (NO ₃) ₇ (CH ₃ OH) ₂]·(NO ₃) (13)	0	17.2 ± 0.2	2.3×10^{-7}			[26]
(NMe ₄) ₂ [Er ₂ Cu ₃ (H ₃ L ⁵) ₂ (NO ₃) ₇ (CH ₃ OH) ₂]·(NO ₃) (14)	0	14.8 ± 0.1	1.2×10^{-7}			[26]
[Cu ₄ Dy ₂ (OH) ₂ (NO ₃) ₈ {(py) ₂ CO ₂ } ₂ (MeCN) ₄] (17)	0	20.1(2)	$8.3(1) \times 10^{-9}$			[27]
[EuCu ₈ (quinha) ₅ (sal) ₂ (py) ₅]·CF ₃ SO ₃ ·py·3H ₂ O (18)	2	21.16	$1.2(5) \times 10^{-7}$			[28]
[{Cu ₅ Tb ₂ (L ⁶) ₂ (μ ₃ -OH) ₄ (ClO ₄)(NO ₃) ₃ (OH ₂) ₅ }·(ClO ₄) ₂ (H ₂ O) _{4.25}] _∞ (21)	0	23.4	1.1×10^{-6}			[29]
[{Cu ₅ Dy ₂ (L ⁶) ₂ (μ ₃ -OH) ₄ (ClO ₄)(NO ₃) ₃ (OH ₂) ₅ }·(ClO ₄) ₂ (H ₂ O) _{5.5}] _∞ (22)	1.2	27.9	6.6×10^{-7}			[29]
[Cu ₄ Dy ₄ (L ⁷) ₄ Cl ₆ (CH ₃ OH) ₈ (H ₂ O) ₄]·Cl ₂ ·(CH ₃ OH) ₉ ·(H ₂ O) ₃ (24)	0	54	2.18×10^{-9}			[30]
[Dy ₂ Cu ₇ (OH) ₂ (L ⁸) ₂ (L ⁹) ₂ (OAc) ₈ (NO ₃) ₂ (H ₂ O) ₄]·(NO ₃) ₂ ·8.5H ₂ O (26)	0	18.0(3)	5.61×10^{-8}			[31]
[DyCu ₈ (OH) ₈ (2-ma) ₈ (Cl) ₂][ClO ₄]·xH ₂ O (29)	0.6	27.0	4.59×10^{-8}			[32]
[ErCu ₈ (OH) ₈ (2-ma) ₈ (Cl) ₂][ClO ₄]·xH ₂ O (30)	0	22.9	4.74×10^{-7}			[32]
[TmCu ₈ (OH) ₈ (2-ma) ₈ (Cl) ₂][ClO ₄]·xH ₂ O (31)	1	33.0	9.48×10^{-6}			[32]
[YbCu ₈ (OH) ₈ (2-ma) ₈ (Cl) ₂][ClO ₄]·xH ₂ O (32)	0.7	24.8	6.50×10^{-6}			[32]
[DyCu ₈ (quinha) ₅ (sal) ₂ (py) ₅]·(CF ₃ SO ₃)·py·4H ₂ O (33)	0	900(31)	$2.0(10) \times 10^{-11}$	20	12	[33]
[Dy ₂ Cu ₁₀ (quinha) ₁₀ (sal) ₂ (OH)(py) ₉]·(CF ₃ SO ₃) ₃ ·2py·2CH ₃ OH·2H ₂ O (34)	0	838(53)	$5(4) \times 10^{-11}$	20	6	[33]
[Dy ₃ Cu ₆ (L ¹⁰) ₆ (μ ₃ -OH) ₆ (H ₂ O) ₁₀]·Cl ₂ ·ClO ₄ ·3.5H ₂ O	0	25	1.5×10^{-7}			[34]
[L ¹¹ Cu(O ₂ COMe)Tb(thd) ₂]	1	13.8	3×10^{-7}	70	0.7	[35]
[Cu ₂ Tb ₂ (L ¹²) ₂ (NO ₃) ₂ (dae-o) ₂]·2(n-BuOH)	0	14.91	2.39×10^{-7}			[36]
	1	23.76	7.00×10^{-8}			[36]

续表

{[CuTb(L ¹²)(n-BuOH) _{0.5}] ₂ (dae-c) ₃ ·5(DMF)·4(n-BuOH)·2(H ₂ O)}	0 1	12.13 22.04	3.03×10^{-6} 2.11×10^{-7}	[36]	
[TbCu(sal)(NO ₃) ₂ (L ¹)(MeOH)]	1	32.9(4)	$3.0(8) \times 10^{-8}$	[37]	
[DyCu(sal)(NO ₃) ₂ (L ¹)(MeOH)]	1	26.0(5)	$1.02(11) \times 10^{-5}$	[37]	
[Cu ₅ Tb ₄ O ₂ (teaH) ₄ {O ₂ CC(CH ₃) ₃ } ₂ (NO ₃) ₄ (OMe) ₄]·2MeOH·2Et ₂ O	0	11.9 ± 0.8	$(9 \pm 6) \times 10^{-6}$	[38]	
[Cu ₅ Dy ₄ O ₂ (teaH) ₄ {O ₂ CC(CH ₃) ₃ } ₂ (NO ₃) ₄ (OMe) ₄]·2MeOH·2Et ₂ O	0	7 ± 1	$(1.3 \pm 0.2) \times 10^{-5}$	[38]	
[Cu ₅ Ho ₄ O ₂ (teaH) ₄ {O ₂ CC(CH ₃) ₃ } ₂ (NO ₃) ₄ (OMe) ₄]·2MeOH·2Et ₂ O	0	10 ± 4	$(3 \pm 2) \times 10^{-6}$	[38]	
[Cu ₅ Dy ₂ (L ⁶) ₂ (μ ₃ -OH) ₄ (μ-H ₂ O) ₂ (μ-OAc) ₂ (OAc) ₂ (OH) ₂] ₂ ·(NO ₃) ₂ ·(H ₂ O) ₂	0 0.9	4 6	3×10^{-6} 3×10^{-6}	[39]	
[Cu ₃ Tb(L ^{Bu})(NO ₃) ₂ (MeOH)(H ₂ O)](NO ₃)·3H ₂ O	0	19.5(5)	3.4×10^{-7}	[40]	
[Dy ₉ Cu ₈ (NO ₃) ₂ (OH) ₁₀ (L ¹³) ₄ (OAc) ₁₈ (H ₂ O) ₄]	0	11.5(4)	1.86×10^{-6}	[41]	
[Cu ₃ Dy ₂ (hfac) ₈ (OH) ₄ (N ₃ tempo)]	4	24	5×10^{-9}	[42]	
[CuDy ₂ (hfac) ₈ (H ₂ O) ₂ (N ₃ tempo) ₂]	4	21	1×10^{-6}	[42]	
[(CuL ¹⁴) ₂ Tb(H ₂ O)(NO ₃) ₃]·MeOH·H ₂ O	1	20.3(7)	$1.5(4) \times 10^{-7}$	[43]	
{[(CuL ¹⁴) ₂ Tb(H ₂ O)(NO ₃) ₃]bpy}·2MeOH·4H ₂ O	1	18.0(10)	$1.2(5) \times 10^{-8}$	[43]	
{[(CuL ¹⁴) ₂ Tb(NO ₃) ₃ bpy]}·MeOH·2H ₂ O _∞	1	23.1(5)	$1.9(4) \times 10^{-9}$	[43]	
[Cu(H ₂ L ¹⁵)(CH ₃ OH)] ₂ Tb(H ₂ O) _{0.57} (DMF) _{0.43} Fe(CN) ₆ ·5.5H ₂ O	2	13	10^{-7}	[44]	
[TbCu ₃ (H ₂ edte) ₃ (NO ₃)][NO ₃] ₂ ·0.5MeOH	0 1	17.3(4) 19.3(1)	$2.2(3) \times 10^{-7}$ $1.4(1) \times 10^{-7}$	140 1.6	[45]
[DyCu ₃ (H ₂ edte) ₃ (NO ₃)][NO ₃] ₂ ·0.5MeOH	1.5	16.2(4)	$1.8(3) \times 10^{-7}$	[45]	
[Cu ₆ Dy ₂ ((L ¹⁶) ³⁻) ₄ (NO ₃) ₃ (OAc)(CH ₃ OH) ₆]·NO ₃ ·OAc·3CH ₃ OH·2H ₂ O	0	5.2	6.5×10^{-6}	[46]	
[Cu ₆ Tb ₂ ((L ¹⁶) ³⁻) ₄ (NO ₃) ₃ (OAc) ₂ (CH ₃ OH) ₅]·NO ₃ ·CH ₃ OH·6H ₂ O	0	15.6(1)	$6.9(2) \times 10^{-7}$	[46]	
[Cu ₄ Dy ₈ (OH) ₆ (NO ₃) ₂ (O ₂ CCH ₂ Bu') ₁₆ (pdm) ₄]	0	7.9(3)	$4.9(4) \times 10^{-7}$	[47]	
[Dy ₂ Cu ₂ (hfac) ₁₀ (NIT-3py) ₂ (H ₂ O) ₂]	0 2	12.51 13.14	8.74×10^{-7} 1.77×10^{-6}	[48]	
[Dy ₄ Cu ₄ (H ₂ L ¹⁷) ₄ Cl ₈ (H ₂ O) ₄] ₂ ·Cl ₄ ·28H ₂ O	0	32.2	8.1×10^{-9}	[49]	
[Cu ₃ Tb(L ^{E1})(NO ₃) ₃ (MeOH)]·MeOH	1	11.3(5)	2.1×10^{-7}	[50]	
[Cu(L ¹⁸)(C ₃ H ₆ O)Dy(NO ₃) ₃]	1	11.42		[51]	
[Cu(L ¹⁸)(C ₃ H ₆ O)Tb(NO ₃) ₃]	1	42.04		[51]	
[Dy ₆ Cu ₆ (H ₂ L ¹⁷) ₆ Cl ₁₂ (H ₂ O) ₆] ₂ ·5ClO ₄ ·OH·30H ₂ O	0	19.6	1.67×10^{-7}	[52]	
[Dy ₄ (H ₂ L ¹⁷) ₄ Cu ₅ (SCN) ₈] ₂	0	11.94	1.52×10^{-6}	[53]	
[Cu ₆ Dy ₁₂ (OH) ₂₀ (N ₃) ₆ (NO ₃) ₈ (dapdo) ₆ (H ₂ O) ₁₈](OH) ₂	0	17	3×10^{-11}	140 1.1	[54]
[Dy ₃ Cu ₂ (HL ¹⁹) ₄ (MeOH)]·ClO ₄	0	7.7	$(2.6 \pm 0.1) \times 10^{-5}$	[55]	
[Dy ₂ Cu ₄ (HL ¹⁹) ₄] ₂ ·(ClO ₄) ₂	0	9.3	$(2.9 \pm 0.2) \times 10^{-7}$	[55]	
[Cu ₅ Dy ₅ (μ ₄ -O)(μ ₃ -OH) ₃ (L ²⁰) ₃ (HL1) ₄ (NO ₃) ₂ (MeOH) ₂] ₂	0.5	8.1	9.7×10^{-7}	[56]	
[Cu ₂ Dy ₂ (μ ₃ -OMe) ₂ (HL ²¹) ₂ (NO ₃) ₄] ₂ ·2MeOH	1.5	16.5	4.5×10^{-7}	[56]	
{[Ho(hfac) ₃] ₂ [Cu(hfac) ₂] ₃ (NIT-Pyrim) ₂ (H ₂ O) ₂ }	0	10.27	6.4×10^{-7}	[57]	

续表

[CuL ^{dpen(1R2R/1S2S)} Tb(NO ₃) ₂] ₂	0	29.4(6)	$1.5(3) \times 10^{-8}$	[58]
[CuL ^{dpen(1R2R/1S2S)} Dy(NO ₃) ₂] ₂	0	13.1(9)	$1.9(7) \times 10^{-7}$	[58]
[DyCu(hfac) ₅ (NIT-Ph-p-OCH ₂ trz)]·0.5C ₆ H ₁₄	0	21.0	5.37×10^{-8}	[59]
[DyCu(hfac) ₅ (NIT-Ph-p-OCH ₂ trz)]	0	29.0	6.1×10^{-10}	[59]
[Cu ₅ Tb ₂ (O ₂ CMe) ₂ (NO ₃) ₄ (L ²²) ₂ (HL ²²) ₂]	0	9.4 ± 0.1	$1.1 \pm 0.2 \times 10^{-7}$	[60]
{[Cu ₅ Dy ₂ (L ²³) ₂ (μ ₃ -OH) ₄ (NO ₃) ₄ (MeOH) ₂ }·(NO ₃) ₂] _∞	0	12	10^{-6}	[61]
[Cu ₂ Dy ₂ (H ₂ L ²⁴) ₂ (L ²⁵) ₂ (OMe)(NO ₃)]·8MeOH	0	8.1	1.4×10^{-5}	[62]
[Cu ₂ Dy ₂ (HL ²⁴) ₂ (L ²⁵) ₂ (MeOH) ₂]·8.5MeOH	0	2.84	1.97×10^{-5}	[62]
[Cu ₂ Tb ₂ (H ₂ L ²⁴) ₂ (L ²⁵) ₂ (H ₂ O)(OMe)(NO ₃)]·0.5H ₂ O·7MeOH	1	8.85	3.2×10^{-7}	[62]
[Dy ₂ Cu ₂ (hfac) ₁₀ (NITPhOPybis) ₂]	0	20.1(4)	$2.0(4) \times 10^{-5}$	[63]
	0.8	21.9(1)	$1.6(9) \times 10^{-5}$	[63]
[Cu ₃ TbCl ₃ (phenox) ₆ (MeOH) ₃]	1	14.4	1.7×10^{-6}	[64]
[Cu ₃ DyCl ₃ (phenox) ₆ (MeOH) ₃]	1	7.7	5.1×10^{-6}	[64]
[Dy ₄ Cu ₄ (H ₂ L ¹⁷) ₄ (H ₂ L ¹⁷) ₄ Cl ₄ (OH) ₄]·Cl ₄ ·24H ₂ O	0	10.6	2.3×10^{-6}	[65]
[Tb ₆ Cu ₆ (H ₂ L ¹⁷) ₆ Cl ₁₂ (H ₂ O) ₆]·5ClO ₄ ·OH·xH ₂ O	0	12.98	1.13×10^{-6}	[66]
[Cu ₃ Ho ₂ (L ²⁶) ₂ (teaH) ₂ (N ₃) ₂ Cl ₂]·3CH ₃ CN	1	4.9	2.0×10^{-6}	[67]
[Cu ₃ Dy ₂ (L ²⁶) ₂ (teaH) ₂ (N ₃) ₂ Cl ₂]·2CH ₃ CN	1	0.7	7.0×10^{-7}	[67]
[Cu ₅ Dy ₂ (O ₂ CMe) ₂ (NO ₃) ₄ (L ²⁷) ₂ (HL ²⁷) ₂ (Me ₂ CO) ₂]	0	13(5)	$1.2(5) \times 10^{-6}$	[68]
[Cu ₅ Dy ₂ (O ₂ CMe) ₂ (NO ₃) ₄ (L ²⁸) ₂ (HL ²⁸) ₂]	0	9.9(4)	$1.2(2) \times 10^{-6}$	[68]
[(CuL ²⁹)Tb(NO ₃) ₃]	2	28.5(5)	$4.1(6) \times 10^{-8}$	[69]
[(CuL ²⁹)Dy(NO ₃) ₃]	2	53(2)	$6(5) \times 10^{-9}$	[69]
[(μ ₄ -CO ₃) ₂ {(CuL ³⁰)(MeOH)Dy(NO ₃) ₂ }]	1.5	6.5	4.2×10^{-7}	[70]
[(μ ₄ -CO ₃) ₂ {(CuL ³⁰)(MeOH)Tb(NO ₃) ₂ }]	1.5	4.5	2.2×10^{-6}	[70]
[Tb ₂ Cu ₃ (hfac) ₁₂ (4-NIT-MePyz) ₄]	2	13	1.84×10^{-7}	[71]
[Dy(hfac) ₃ Cu(hfac) ₂ (bisNITPhPyrim)]	0.5	8.13	1.07×10^{-6}	[72]
[Tb(H ₂ O) ₃ {Cu(pyzha)} ₅ (H ₂ O) ₃](TfO) ₂ ·3(H ₂ O)·(MeOH)	0	5.42	8.09×10^{-7}	[73]
[Yb{Cu ₄ (butyrat) ₄ } ₂]·Cl ₃ ·MeOH·26H ₂ O	1	6.84	1.04×10^{-5}	[74]
[CuL ³¹ (μ-NO ₃)Tb(NO ₃) ₂ (H ₂ O)]·CH ₃ CN	2	19.3(8)	$8(2) \times 10^{-8}$	[75]
[CuL ³¹ (μ-NO ₃)Dy(NO ₃) ₂ (H ₂ O)]·CH ₃ CN	2	26.1(10)	$1.6(5) \times 10^{-8}$	[75]
[CuL ³² (μ-NO ₃)Tb(NO ₃) ₂ (H ₂ O)]·CH ₃ CN	2	23.8(10)	$9.1(39) \times 10^{-10}$	[75]
[CuL ³² (μ-NO ₃)Dy(NO ₃) ₂ (H ₂ O)]·CH ₃ CN	2	28.2(5)	$7.2(9) \times 10^{-8}$	[75]
[HoCu(hfac) ₅ NIT-Ph-p-OCH ₂ trz]·0.5C ₆ H ₁₄] _n	2	4.93	1.64×10^{-6}	[76]
[[CuL ³³]Ln(NO ₃) ₃ ·H ₂ O]·CH ₃ CN	5	15.4	2.15×10^{-6}	[77]
[[CuL ³⁴]Ln(NO ₃) ₃ ·H ₂ O]·CH ₃ CN	5	17.9	1.1×10^{-6}	[77]
[Dy ₂ Cu ₂ (hfac) ₁₀ (PPNIT) ₂ (H ₂ O) ₂]·CHCl ₃	1.5	17.8 (6)	$3.4(3) \times 10^{-6}$	[78]
[Cu(Cl)(valen)Tb(NO ₃)(CH ₃ OH)(H ₂ O)(dca)]	0	21.85	7.65×10^{-4}	[79]
[LnCu(hfac) ₅ NIT-Ph-p-OCH ₂ trz] _n	0	7.3	2.93×10^{-6}	[80]
[(L ³⁵) ₃ Cu ₃ TbCl ₂ (NO ₃) ₂ (H ₂ O) ₂]	0	10.49(8)	$5.02(14) \times 10^{-8}$	[81]
	1	13.3(2)	$3.1(2) \times 10^{-8}$	[81]

续表

$[(L^{35})_3Cu_3Gd(NO_3)_2(H_2O)_2(MeOH)](NO_3)$	2	10.8(2)	$8.8(6) \times 10^{-8}$	[81]
$[(L^{35})_3Cu_3Dy(NO_3)_2(H_2O)_2(MeOH)](NO_3)$	1	7.82(4)	$6.05(11) \times 10^{-8}$	[81]
$[Cu_6Dy_3(R-L^{36})_6(OH)_6(H_2O)_6](ClO_4)(NO_3)_2 \cdot 4.75H_2O \cdot 0.8MeOH$	0	19.5(0.6)	$4.1(0.1) \times 10^{-8}$	[82]
$[Cu_6Dy_3(S-L^{36})_6(OH)_6(H_2O)_6](ClO_4)(NO_3)_2 \cdot 5.5H_2O \cdot 0.8MeOH$	0	21.4(0.4)	$2.7(0.1) \times 10^{-8}$	[82]
H2L1 = 2, 2-dimethyl-N, N-bis(3-methoxysalicylal)-1, 3-propanediamine; o-vanilate = 2-hydroxy-3-(methoxybenzaldehyde); H2L2 = N, N'-bis(3-methoxysalicylidene)-1, 3-diamino-2, 2-dimethylpropane; H2valpn = 1, 3-propanediylbis(2-iminomethylene-6-methoxyphenol); H2L3 = N, N'-bis(3-methoxysalicylidene)-2, 2-dimethylpropane-1, 3-diamine; H3L4 = 1-(2hydroxybenzamido)-2-(2-hydroxy-3-methoxybenzylideneamino)ethane; Hhfac = hexafluoroacetylacetone; dpk- = di-2-pyridyl ketoximate; H6L5 = 2, 2'-(propane-1, 3-diylidimino)bis[2-(hydroxymethyl)propane-1]; H3L6 = N, N'-bis(3-methoxysalicylidene)-1, 3-diamino-2-propanol; 2-ma = 2-methylalanine; (py)2CO = di-2-pyridyl ketone; H3L7 = 2-[2-(2-hydroxy-3-methoxybenzylidene)-hydrazineyl]-2-oxo-N-(pyridin-2-ylmethyl)acetamide; H2quinha = quinaldichydroxamic acid; Hsal = salicylaldehyde; py = pyridine; L8 = hydroxy(pyridin-2-yl)methanolate; L9 = (S)-((R)-hydroxy(pyridin-2-yl)methoxy)(pyridin-2-yl)methanolate; H2L10 = 1, 1, 1-trifluoro-7-hydroxy-4-methyl-5-azahept-3-en-2-one; (L11)2- = N, N'-2, 2-dimethylpropylenedi(3-methoxysalicylideneiminato); thd = tetramethylheptanedionato; H2L12 = 1, 3-bis((3-methoxysalicylidene)amino)propane; H2dae = 1, 2-bis(5-carboxyl-2-methyl-3-thienyl)perfluoropentene; teaH3 = triethanolamine; H6LBu = (2E, 8E, 11E, 17E, 20E, 26E)-3, 8, 12, 17, 21, 26-hexaaza-1, 10, 19(1, 4)-tribenzenacycloheptacosaphane-2, 8, 11, 17, 20, 26-hexaene-12, 13, 102, 103-tetraol; H2L13 = (Z)-1, 3-di(pyridin-2-yl)but-1-ene-1, 3-diol; N3tempo = 4-azido-2, 2, 6, 6-tetramethylpiperidine-1-oxyl radical; H2L14 = N, N'-bis(salicylidene)-1, 3-propanediamine; bpy = 4, 4'-bipyridine; H4L15 = N, N'-ethylenebis(3-hydroxysalicylidene); H4edte = 2, 2', 2'', 2'''-(ethane-1, 2-diyl)dinitrilo)tetraethanol; (L16)3- = in situ prepared acylhydrazone ligand; pdmH2 = pyridine-2, 6-dimethanol; ButCH2CO2- = tert-butylacetate ion; NIT-3py = 2-(3-pyridyl)-4, 4, 5, 5-tetramethylimidazoline-1-oxyl-3-oxide; H4L17 = tritopic hydrazone ligand; tpa = terephthalate; H6LEt = [3+3] imine macrocycle derived from 1, 4-diformyl-2, 3-dihydroxybenzene and 1, 2-diaminoethane; H2L18 = N, N'-bis(3-methoxysalicylidene)-1, 3-diamino-2, 2-dimethylpropane; dapdoH2 = 2, 6-diacetylpyridine dioxime; H4L19 = 2, 2'-{2-hydroxy-3-[2-hydroxyphenylimino]methyl}-5-methylbenzylazanediyl}diethanol; H3L21 = (E)-2-((2-hydroxy-3-methoxybenzylidene)amino)propane-1, 3-diol; H3L22 = (E)-2-ethyl-2-((2-hydroxy-3-methoxybenzylidene)amino)propane-1, 3-diol; NIT-Pyrim = 2-(5-pyrimidinyl)-4, 4, 5, 5-tetramethylimidazoline-1-oxyl-3-oxide; H3Lopen(1R2R) = N-((1R, 2R)-2-(((E)-3-Ethoxy-2-hydroxybenzylidene)amino)-1, 2-diphenylethyl)-2-hydroxybenzamide; NIT-Ph-p-OCH2trz = 2-[4-[(1H-1, 2, 4-triazol-1-yl)methoxy]phenyl]-4, 4, 5, 5-tetramethylimidazoline-1-oxyl-3-oxide; hfac = hexafluoroacetylacetone; H3L21 = OH-C10H7-CH=NC(C2H5)(CH2OH)2; H3L23 = N, N'-bis(3-methoxysalicylidene)-1, 3-diamino-2-propanol; H4L24 = butanedihydrazide-bridged bis(3-ethoxysalicylaldehyde); H2L25 = 2-salicylideneaminophenol; NITPhOPybis = 5-(4-oxyppyridinium-1-yl)-1, 3-bis(1'-oxyl-3'-oxido-4', 4', 5', 5'-tetramethyl-4, 5-hydro-1H-imidazol-2-yl)benzene; phenoxH = hrendione-9-oxime; H2L26 = N1, N3-bis(3-methoxysalicylidene)diethylenetriamine; H2L27 = OH-C10H6-CH=NC(CH3)(CH2OH)2; H2L28 = OH-C10H6-CH=NC(C2H5)(CH2OH)2; H2L29 = N-a-methylsalicylidene-N'-3-methoxysalicylidene-1, 3-propanediamine; H2L30 = N-3-ethoxysalicylidene-N'-3-methoxysalicylidene-1, 3-propanediamine; 4-NIT-MePyz = 2-{4-(1-methyl)-pyrazolyl}-4, 4, 5, 5-tetramethylimidazoline-1-oxyl-3-oxide; bisNITPhPyrim = 5-(5-pyrimidyl)-1, 3-bis(1'-oxyl-3'-oxido-4', 4', 5', 5'-tetramethyl-4, 5-hydro-1H-imidazol-2-yl)benzene; TfO = trifluoromethanesulfonate; H2pyzha = pyrazinehydroxamic acid; H2butyrat = 3-aminobutyric hydroxamic acid; H2L31 = N-salicylidene-N'-3-ethoxysalicylidene-1, 3-propanediamine; H2L32 = N-salicylidene-N'-3-methoxysalicylidene-1, 3-propanediamine;; H2L34 = N-Salicylidene-N'-3-methoxysalicylidene-1, 2-diamine; PPNIT = 2-(1-(pyrazin-2-yl)-1H-pyrazole)-4, 4, 5, 5-tetramethyl-imidazoline-1-oxyl-3-oxide; H2valen = 1, 2-ethanediylbis(2-iminomethylene-6-methoxy-phenol); dca = dicyanamide; H2L35 = diformylnaphthalene-2, 3-diol; R-H2L36 = 1-((E)-(((1R, 2R)-2-hydroxycyclohexyl)imino)methyl)naphthalen-2-ol; S-H2L36 = 1-((E)-(((1S, 2S)-2-hydroxycyclohexyl)imino)methyl)naphthalen-2-ol				

2009 年, Takashi Kajiwara 及其同事报道了两种配合物, $[TbCu(L^1)(NO_3)_3(H_2O)]$ (**1**, $H_2L^1 = 2$, 2-dimethyl-N,N-bis(3-methoxysalicylal)-1,3-propanediamine)和 $[TbCu(L^1)(o\text{-vanilate})(NO_3)(MeOH)]NO_3$ (**2**)。在这两种配合物中, 席夫碱配体(L^1)²⁻为 Cu^{II} 和 Tb^{III} 提供近乎共面的配位原子 N_2O_2 和 O_4 , 分别与两个苯氧基桥接了 Cu^{II} 和 Tb^{III} 。因此, **1** 和 **2** 中的 $[TbCu(L^1)]^{3+}$ 部分表现出显著的结构相似性(图 1)。直

流磁化率测量表明，两种配合物的铁磁相互作用较弱，同时观察到 Tb^{III} 具有显著的磁各向异性。交流磁化率测试分别在低于 5 K 和 6 K 的温度下，观察到了 **1** 和 **2** 的 SMM 行为。将数据拟合到阿伦尼乌斯方程中，**1** 和 **2** 的有效能垒 Δ/k_{B} 分别为 29(2) K 和 32.2(6) K (图 2)。此外，DFT 计算表明，由于在与 $\text{Tb}^{\text{(III)}}$ 桥接的苯氧原子相反的位置引入了苯氧配体，导致负电荷的单轴排列，从而增强了 Tb^{III} 的轴向磁各向异性，配合物 **2** 具有更大的有效能垒[20]。

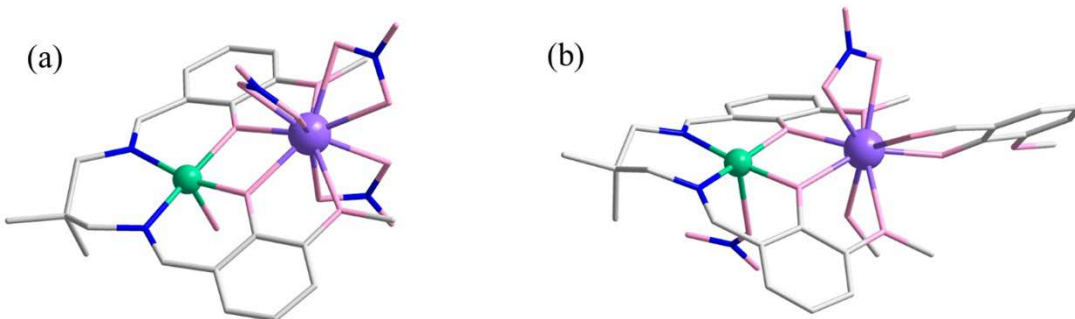


Figure 1. The molecular structure of **1** (a) and **2** (b). Color code: Cu^{II} , green; Tb^{III} , purple; O, pink; N, blue; C, gray. H atoms are omitted for clarity. Reproduced from [20]
图 1. **1** (a)和 **2** (b)的分子结构图。颜色： Cu^{II} ，绿色； Tb^{III} ，紫色；O，粉红色；N，蓝色；C，灰色。为清楚起见，省略了H原子。转载自[20]

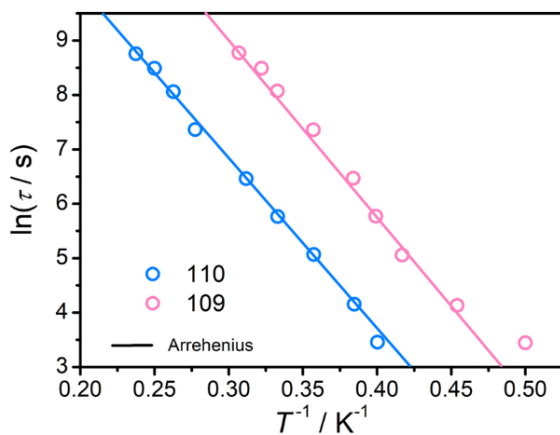


Figure 2. Arrhenius plots of **1** (a) and **2** (b). The solid line represents the fitting curves with the Arrhenius law. Reproduced from [20]
图 2. **1**(a)和 **2**(b)的阿伦尼乌斯图。实线代表了阿伦尼乌斯定律的拟合曲线。转载自[20]

2012 年，Takayuki Ishida 及其同事合成了一类配合物 $[\text{Cu}^{\text{II}}(\text{L}^2)(\text{C}_3\text{H}_6\text{O})\text{Ln}^{\text{III}}(\text{NO}_3)_3]$ ($\text{Ln} = \text{Tb}$ (**3**), Dy (**4**)), $\text{H}_2\text{L}^2 = \text{N}, \text{N}'\text{-bis}(3\text{-methoxysalicylidene})\text{-1, 3-diamino-2, 2-dimethylpropane}$)。在这些配合物中， Cu^{II} 在赤道方向上与来自席夫碱配体(L^2)²⁻的两个亚胺氮原子和两个苯氧化氧原子配位，并在轴向上与一个丙酮分子配位，从而形成四方金字塔构型(图 3)。 Ln^{III} 与 6 个硝酸盐氧原子、2 个甲醇氧原子和 2 个酚酸盐氧原子配位，形成具有 10 个配位点的配位环境。配合物 **3** 在 2 K 以上表现出明显的频率依赖性，当施加 1 kOe 的外部磁场时，QTM 被有效抑制，使频率依赖性更加明显。磁化反转的能垒确定为 $E_a/k_{\text{B}} = 42.3(4)$ K，指前因子 $\tau_0 = 7.1(9) \times 10^{-10}$ s。另一方面，配合物 **4** 在 1 kOe 的外部磁场下也表现出频率依赖性，通过拟合阿伦尼乌斯定律，确定其磁各向异性势垒为 11.5 (10) K [21]。

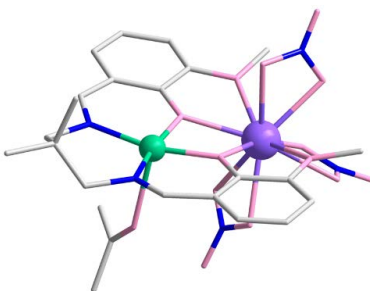


Figure 3. The molecular structure of **3**. Color code: Cu^{II}, green; Tb^{III}, purple; O, pink; N, blue; C, gray. H atoms are omitted for clarity. Reproduced from [21]

图 3. 配合物 **3** 的分子结构图。颜色：Cu^{II}，绿色；Tb^{III}，紫色；O，粉红色；N，蓝色；C，灰色。为清楚起见，省略了H原子。转载自[21]

2006年，Takayuki Ishida 及其同事报道了氧化物桥接三核配合物[(Dy(hfac)₃)₂Cu(dpk)₂] (**5**, Hdpk = di-2-pyridyl ketoxinate)的例子。在这个配合物中，两个 dpk⁻配体桥接两个 Dy^{III}离子和一个 Cu^{II}离子，导致三个金属离子的线性排列。Cu^{II}采用方形平面构型，由来自两个 dpk⁻基团的4个N原子进行配位。除了来自三个 hfac⁻的六个氧原子外，Dy^{III}还与来自 dpk⁻的一个N原子和一个O原子配位，从而产生了八配位构型(图 4)。在交流磁化率测量中，**5** 的实部和虚部信号都表现出明显的频率依赖性，有效能量势垒 $\Delta/k_B = 47(4)$ K，指前因子 $\tau_0 = 1.1(5) \times 10^{-7}$ s。推测 **5** 的SMM行为源于 Dy^{III}的单离子各向异性，以及 Dy^{III}和 Cu^{II}之间的强耦合[22]。

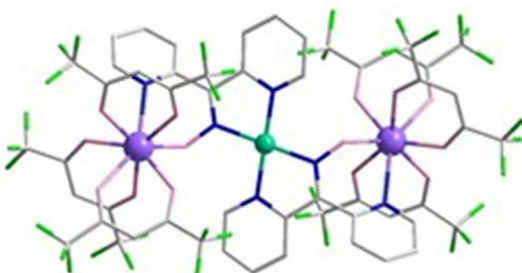


Figure 4. The molecular structure of **5**. Color code: Cu^{II}, green; Tb^{III}, purple; O, pink; N, blue; C, gray; F, bright green. H atoms are omitted for clarity. Reprinted with permission from Ref. [22]. Copyright 2006 American Chemical Society

图 4. 配合物 **5** 的分子结构图。颜色：Cu^{II}，绿色；Tb^{III}，紫色；O，粉红色；N，蓝色；C，灰色；F，亮绿色。为清楚起见，省略了H原子。经参考文献[22]许可转载。版权所有 2006 美国化学学会

2024年，Wen-Bin Sun 及其同事报道了一种配合物，[Cu₂(L³)₂DyCl₂(H₂O)]·Cl·MeCN (**6**)，(L³ = N,N'-bis(3-methoxysalicylidene)-2,2-dimethylpropane-1,3-diamine)。这种配合物具有线性 Cu-Dy-Cu 型配位结构，对配合物中异常离子周围局部配位环境的分析表明，它采用九配位构型(图 5)。Cu (II)离子形成键的苯氧基氧原子沿着 Cu-Dy-Cu 轴呈现一个方向，而外部的甲氧基氧原子通常采用一个垂直于 Cu-Dy-Cu 的方向。每个席夫碱前驱体贡献了四个配位氧原子。直流磁化率测试表明，在 300 K~50 K 的温度范围内，配合物的磁化率保持相对稳定。在 50 K 以下，配合物快速增加趋势，在 4 K 时达到最大值，然后逐渐下降到 2 K。交流磁化率中，配合物在零场下表现出明显的温度依赖行为，最高峰值温度为 10.5 K，频率为 999 Hz，表现出典型的单分子磁体行为。此外通过磁滞回线的测量，发现最大磁滞开口温度为 3.5 K，这与在零直流场下交流磁化率中观察到的显著磁弛豫行为一致。通过拟合阿伦尼乌斯方程得到，配合物的

有效能垒是 39.06 K, $\tau_0 = 1.05 \times 10^{-5}$ s。

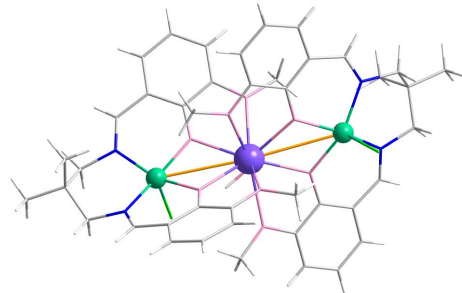


Figure 5. The molecular structure of **6**. Color code: Cu^{II}, green; Tb^{III}, purple; O, pink; N, blue; C, gray. H atoms are omitted for clarity

图 5. 配合物 **6** 分子结构图。颜色：Cu^{II}，绿色；Tb^{III}，紫色；O，粉红色；N，蓝色；C，灰色。为清楚起见，省略了H原子

2003 年, Shutaro Osa 等人报道了有关 3d-4f SMM 的第一个实例, [Cu^{II}(L⁴Tb^{III}(hfac)₂)₂(7,L⁴ = 1-(2hydroxybenzamido)-2-(2-hydroxy-3-methoxy-benzylideneamino) ethane, Hhfac = hexafluoroacetylacetone)。该配合物采用四核环状结构, Cu^{II}和 Tb^{III}离子交替排列。Cu^{II}离子表现出由 H₃L⁴ 体提供的 N₂O₂ 供体原子形成的方形平面配位几何形状, 而 Tb^{III}离子实现了八面体配位, 是由两个 hfac⁻的四个氧原子和来自两个(L⁴⁻)的四个氧原子形成的(图 6)。流磁化率表明 Cu^{II}和 Tb^{III}离子之间存在铁磁相互作用。交流磁化率中 **7** 的虚部信号显示出了明显的频率依赖性, 证实了该配合物存在单分子磁体行为。该配合物的有效能垒 Δ/k_B 是 21 K, 指前因子 τ_0 为 2.7×10^{-8} s [24]。

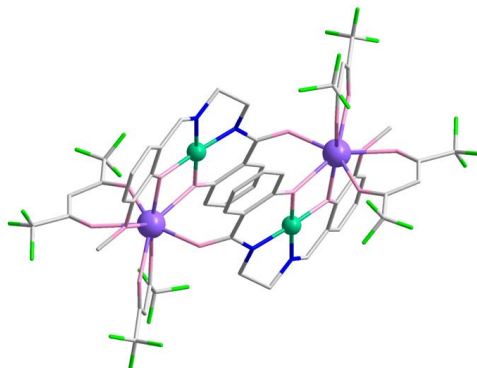


Figure 6. The molecular structure of **6**. Color code: Cu^{II}, green; Tb^{III}, purple; O, pink; N, blue; C, gray; F, bright green. H atoms are omitted for clarity. Reprinted with permission from Ref. [24]. Copyright 2003 American Chemical Society.

图 6. 配合物 **6** 的分子结构图。颜色：Cu^{II}，绿色；Tb^{III}，紫色；O，粉红色；N，蓝色；C，灰色；F，亮绿色。为清楚起见，省略了H原子。经参考文献[24]许可转载。

版权所有 2003 美国化学学会

2013 年, 由 Xin-Yi Wang 领导的研究小组报道了两个末端叠氮基桥接四核配合物的例子, [Cu₂(valpn)₂Tb₂(N₃)₆]·2CH₃OH(**8**, H₂valpn = 1,3-propanediylbis(2-iminomethylene-6-methoxyphenol))。两个 [CuTb] 单元由两个末端的 N₃⁻ 配体桥接, 形成[Cu₂Tb₂]簇(图 7(a))。在每个[CuTb] 单元内, valpn²⁻ 配体给 Cu^{II} 和 Tb^{III} 离子分别提供了具有 N₂O₂ 和 O₄ 的配位环境。同时, 其余 4 个 N₃⁻ 配体也参与 Tb^{III} 和 Cu^{II} 的配位环境, 导致 Cu^{II} 形成细长八面体构型, Ln^{III} 形成八配位三角棱柱几何构型。在零外加直流场下对配合

物进行交流磁化率的测量，结果表明，**7**表现出 SMM 行为，有效能量势垒为 $U_{\text{eff}} = 30.1 \pm 0.7$ K。此外，在扫描速率为 0.05 Ts^{-1} 时，**8** 的磁滞回路的开启温度为 2.4 K (图 7(b)) [25]。

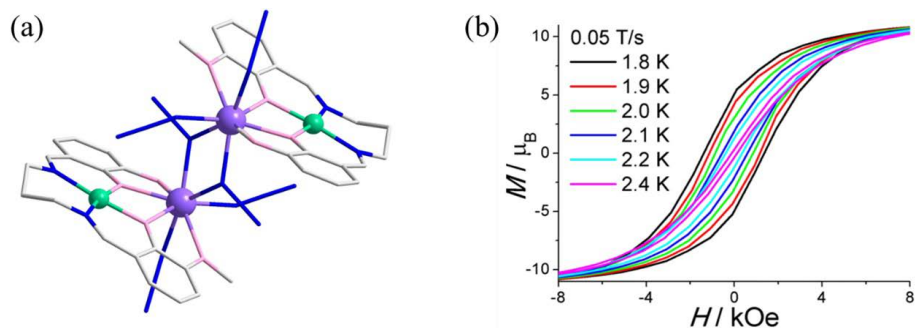


Figure 7. The molecular structure (a) and magnetic hysteresis (b) of **8**. Color code: Cu^{II}, green; Dy^{III}, purple; O, pink; N, blue; C, gray. H atoms are omitted for clarity. Reproduced from [25]

图 7. 配合物 **8** 的分子结构图(a)和磁滞回线图(b)。颜色：Cu^{II}，绿色；Dy^{III}，紫色；O，粉红色；N，蓝色；C，灰色。为清楚起见，省略了 H 原子。转载自[25]

2016 年，Mark Murrie 等人报道了一系列的 3d-4f 配合物，即 $[\text{Ln}_2\text{Cu}_3(\text{H}_3\text{L}^5)_2(\text{CH}_3\text{COO})_6]$ ($\text{Ln} = \text{Gd}$ (**9**), Tb (**10**) $\text{H}_6\text{L}^5 = 2, 2'-(\text{propane}-1, 3\text{-diyldiimino}) \text{ bis}[2-(\text{hydroxymethyl}) \text{ propane}-1, 3\text{-diol}]$) 和 $[\text{Ln}_2\text{Cu}_3(\text{H}_3\text{L}^5)_2(\text{NO}_3)_7(\text{CH}_3\text{OH})_2]$ ($\text{Ln} = \text{Tb}$ (**11**), Dy (**12**), Ho (**13**), Er (**14**))。**化合物 9-10** 是同构而 **11-14** 也表现出同构特征。在 **9-10** 中，两个去质子化配体 $(\text{H}_3\text{L}^5)^3-$ 提供四个 μ -O 桥和两个 μ_3 -O 桥，将两个 Ln^{III} 离子连接到线性单元 $[\text{Cu}_3(\text{H}_3\text{L}^5)_2]$ (图 8(a))。此外，这两个 $(\text{H}_3\text{L}^5)^3-$ 配体将两个外 Cu^{II} 离子包封在线性单元中，这就导致了外部的 Cu^{II} 离子是扭曲方棱锥几何结构，而中心 Cu^{II} 离子是扭曲八面体构型。 Ln^{III} 离子的配位环境与球形帽盖正方形反棱镜非常相似(图 9(a)，插图)。**11-14** 的核心结构与 **9-10** 有相似之处，由两个 Ln^{III} 离子和一个线性单元组成(图 8(b))。区别在于存在与外部 Cu^{II} 离子配位的单齿 NO_3^- ，形成扭曲的八面体构型。此外，两个双齿和一个单齿 NO_3^- 配体与 MeOH 一起参与了两个 Ln^{III} 离子的配位环境。因此，两个 Ln^{III} 离子分别表现出球形带端正方形反棱镜和松饼状配位几何形状(图 9(b)，插图)。通过与阿伦尼乌斯定律的拟合，确定 **10** 和 **11** 的有效能垒分别为 21.4 K 和 36.0 K (图 9)。由于配合物 **12-14** 的交流磁化率信号中没有峰值，因此使用 $\ln(\chi''/\chi') = \ln(2\pi\nu\tau_0) + U_{\text{eff}}/k_B T$ 模型，粗略估计它们的能量分别为 23.9 K、17.2 K 和 14.8 K。对 **10** 和 **11** 的理论计算表明，它们势垒的差异可能源于不同的 Ln^{III} 协调环境。此外， Cu^{II} 和 Tb^{III} 之间的磁交换相互作用可以有效地抑制 QTM，从而可以观察 SMM 在零场条件下的行为[26]。

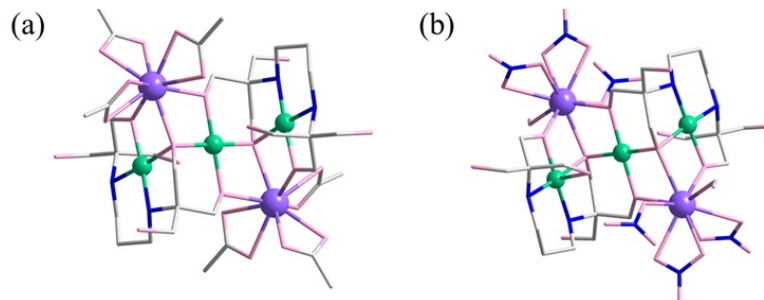


Figure 8. The molecular structure of **10** (a) and **11** (b). Color code: Cu^{II}, green; Tb^{III}, purple; O, pink; N, blue; C, gray. H atoms are omitted for clarity. Reproduced from [26]

图 8. **10** (a) 和 **11** (b) 的分子结构。颜色：Cu^{II}，绿色；Tb^{III}，紫色；O，粉红色；N，蓝色；C，灰色。为了清楚起见省略了 H 原子。转载自[26]

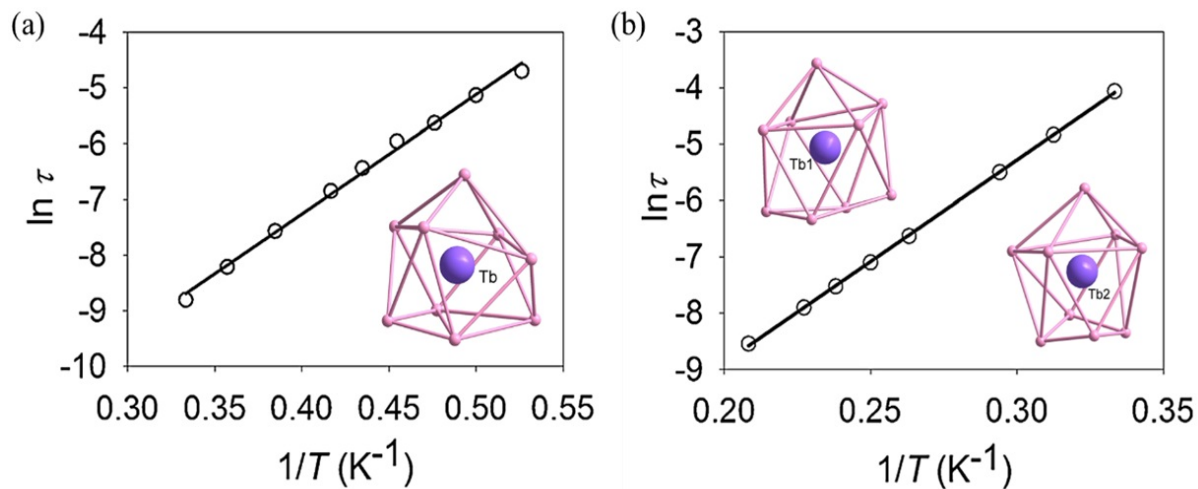


Figure 9. Magnetization relaxation time $\ln(\tau)$ vs T^{-1} plot for **10** (a) and **11** (b). The solid line is fitting curve with the Arrhenius law. Inset: The coordination environment of Ln^{III} in **10** (a) and **11** (b). Reproduced from [26]

图 9. **10** (a) 和 **11** (b) 的磁化弛豫时间 $\ln(\tau)$ 与 T^{-1} 的关系图。实线是阿伦尼乌斯定律的拟合曲线。插图: Ln^{III} 在 **10** (a) 和 **11** (b) 中的配位环境。转载自[26]

2018年, Theocharis C. S.及其同事报道了一系列Cu-Ln簇,即 $[\text{Cu}_4\text{Ln}_2(\text{OH})_2(\text{NO}_3)_8\{\text{(py)}_2\text{CO}_2\}_2(\text{MeCN})_4]$ ($\text{Ln} = \text{Gd}$ (**15**), Tb (**16**),和 Dy (**17**))。这三种配合物表现出结构相似性,因为它们都由两个三角形 $[\text{Cu}_2\text{Ln}(\mu_3\text{-OH})]^{6+}$ 单元组成,这两个单元由两个 $(\text{py})_2\text{CO}_2^{2-}$ 配体的醇盐臂桥接。在对称相关的 $[\text{Cu}_2\text{Ln}(\mu_3\text{-OH})]^{6+}$ 单元中, $\mu_3\text{-OH}^-$ 位于 $[\text{Cu}_2\text{Ln}]$ 平面上方,导致四面体几何形状扭曲(图 10(a), 插图)。配合物 **15**在交流磁化率测量中仅显示出与频率相关的虚部信号的尾部,使得难以获得其各向异性值。相反,化合物 **16**在4 K以下表现出明显的频率依赖性信号,拟合这些数据得到20.1(2) K的有效能垒(图 10(a))。值得注意的是,配合物 **16**在 Cole-Cole 图中显示出宽的弛豫时间分布,这可归因于 QTM 和热激活弛豫过程的综合效应(图 10(b)) [27]。

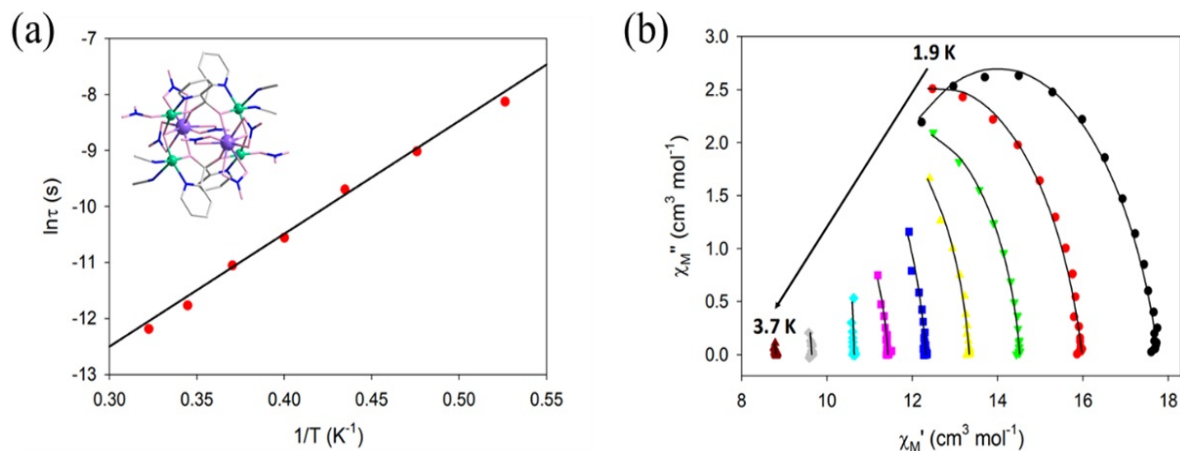


Figure 10. The Arrhenius plot for complex **17** under zero dc field (a) and Cole-Cole plots for complex **17** (b). Inset: The molecular structure of **17**. Color code: Cu^{II}, green; Dy, purple; O, pink; N, blue; C, gray. The solid line corresponds to the fit of the data. H atoms are omitted for clarity. Reproduced from [27]

图 10. 配合物 **17** 在零直流场下的 Arrhenius 图(a), 插图: **17** 的分子结构, 和配合物 **17** 的 Cole-Cole 图(b)。颜色: Cu^{II}, 绿色; Dy, 紫色; O, 粉红色; N, 蓝色; C, 灰色。实线对应于数据的拟合。为了清楚起见省略了H原子。转载自[27]

2019 年，报道了一种杂金属冠醚化合物，表示为 $[\text{EuCu}_5(\text{quinha})_5(\text{sal})_2(\text{py})_5] \cdot \text{CF}_3\text{SO}_3 \cdot \text{py} \cdot 3\text{H}_2\text{O}$ (**18**)。 H_2quinha = quinaldichydroxamic acid, Hsal = salicylaldehyde, py = pyridine)。在该配合物中， Eu^{III} 离子被包裹在 $[\text{MCu}_{II}-5]$ 内，与 Hsal 配体衍生的两个苯氧基氧原子形成轴向配位。这种排列导致 Eu^{III} 周围的配位几何结构非常类似于扭曲的五角双锥。 $[\text{MCu}_{II}-5]$ 单元由五个完全去质子化的 quinha^2- 配体组成，与五个 Cu^{II} 离子配位，采用 $\mu_3: \eta^2: \eta^2: \eta^1$ 配位模式(图 11(a))。磁化率测量显示 **18** 在零磁场条件下没有任何显示与频率相关的虚部信号。然而，在施加 2 kOe 的外部磁场时，它表现出缓慢的磁弛豫行为。使用 $\tau^{-1} = CT^n$ 拟合 **18** 的弛豫时间，并确定 **18** 中的主要弛豫过程是拉曼过程，源于 $\{\text{Cu}_5\}$ 团簇的 $S = 1/2$ 基态。当用抗磁性离子 Lu^{III} (**19**)和 Y^{III} (**20**)取代 Eu^{III} 时，两种配合物在 2 kOe 的外磁场下表现出相似的磁性行为(图 11(b))。然而，观察到 **18** 的弛豫时间比 Lu^{III} 和 Y^{III} 类似物的弛豫短。这种现象可归因于 Eu^{III} 离子基态产生的二阶效应或声子瓶颈效应的存在[28]。

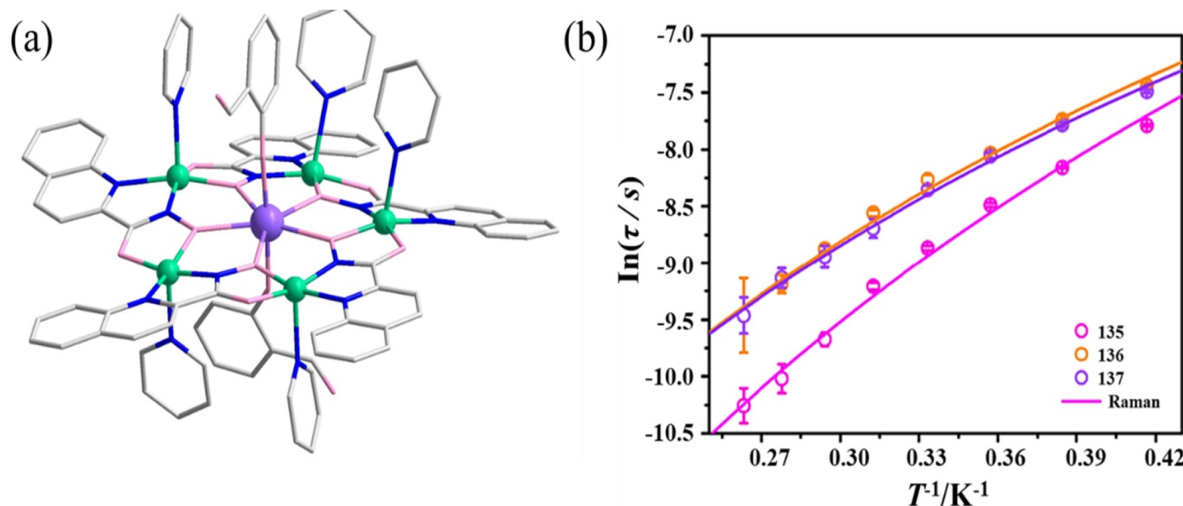


Figure 11. The molecular structure for **18** (a) and the temperature-dependence of relaxation times for **18-20** under a 2 kOe DC field (b). Color code: Cu^{II} , green; Eu , purple; O, pink; N, blue; C, gray. H atoms are omitted for clarity. The solid line corresponds to the fit of the data. Reproduced from [28]

图 11. **18** 的分子结构图(a)和 **18-20** 在 2 kOe 直流场下的温度依赖的弛豫时间(b)。颜色： Cu^{II} ，绿色； Eu ，紫色；O、粉红色；N、蓝色；C、灰色。为了清楚起见省略了 H 原子。实线对应于数据的拟合。转载自[28]

2017 年，Vadapalli-Chandrasekhar 及其同事合成了一系列一维单分子磁体，表示为 $[\{\text{Cu}_5\text{Ln}_2(\text{L}^6)_2(\mu_3-\text{OH})_4(\text{ClO}_4)_4(\text{NO}_3)_3(\text{OH}_2)(\text{ClO}_4)_2(\text{H}_2\text{O})_x\}]_x$ ($\text{Ln} = \text{Tb}$ (**21**)、 Dy (**22**)和 Ho (**23**)，分别为 **21-23** 的 $x = 4.25$ 、 5.5 和 5 ， $\text{H}_3\text{L}^6 = \text{N}, \text{N}'\text{-bis}(3\text{-methoxysalicylidene)}\text{-1, 3-diamino-2-propanol}$)。配合物 **21-23** 表现出同构性，但具有不同数量的间隙水分子。在单元 A 中，外部的四个 Cu^{II} 离子和两个 Ln^{III} 离子通过两个 $(\text{L}^6)^3-$ 配体和两个 $\mu: \eta^1: \eta^1-\text{NO}_3^-$ 配体相互连接，而中心的 Cu^{II} 离子通过四个 $\mu_3\text{-OH}^-$ 和两个 $\mu: \eta^2-\text{NO}_3^-$ 配体与周围的六个金属离子连接。除了上述配位基团外，水分子还参与了 Ln^{III} 离子的配位环境。此外， $\mu_3: \eta^2: \eta^1-\text{NO}_3^-$ 配体桥接类似的七核单元(单元 B)，从而形成整体的一维结构(图 12(a))。磁化率测量证实了化合物 **21-23** 的 SMM 行为。化合物 **21** 表现出两种弛豫模式，这可能归因于一维结构中存在两个不同的单元。通过阿伦尼乌斯定律拟合，确定了 3 K 以上热激活弛豫过程的能量为 23.4 K。在较低的温度下，QTM 主导弛豫机制，但在施加 1.2 kOe 的外部磁场时，有效能垒增加到 27.9 K(图 12(b))。对于高于 3 K 的热激活弛豫过程，化合物 **22** 表现出 8.3 K 的有效能垒，而化合物 **23** 表现出低于 4 K 的快速 QTM，阻碍了预估的 SMM 能垒[29]。

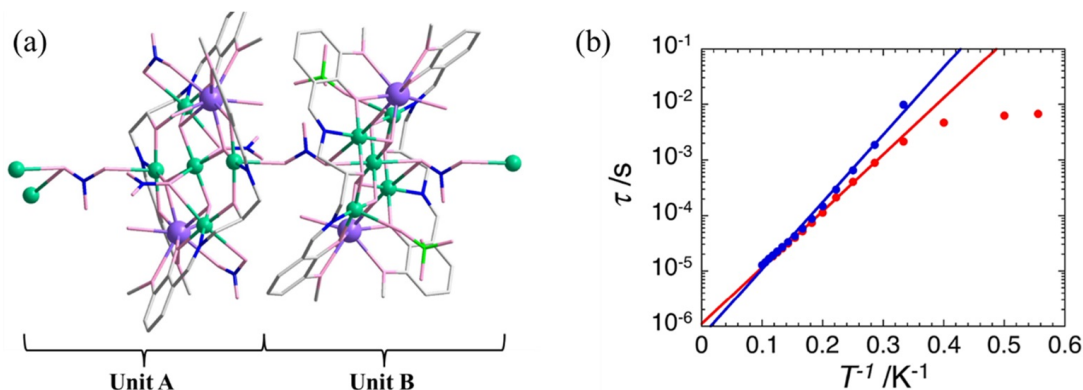


Figure 12. The structure of two $[\text{Cu}_5\text{Tb}_2]$ repeating units in the 1D coordination assembly **21** (a) and temperature dependence of the magnetization relaxation time as τ versus T^{-1} plot for **21** in zero (red) and 1200 Oe (blue) dc field. Color code: Cu^{II} , green; Tb^{III} , purple; O, pink; N, blue; C, gray; Cl, bright green. H atoms are omitted for clarity. Reprinted with permission from Ref. [29]. Copyright 2013 American Chemical Society

图 12. 一维的配位组件 **21(a)** 中两个 $[\text{Cu}_5\text{Tb}_2]$ 重复单元的结构以及 **21** 在零(红色)和 1200 Oe (蓝色)直流场中磁化弛豫时间的温度依赖性 τ 与 T^{-1} 的关系图。颜色: Cu^{II} , 绿色; Tb^{III} , 紫色; O、粉红色; N、蓝色; C、灰色; Cl, 亮绿色。为了清楚起见省略了 H 原子。经参考文献[29]转载。版权所有 2013 美国化学学会

2019 年, 刘伟胜领导的课题组合成了两种八核配合物, $[\text{Cu}_4\text{Dy}_4(\text{L}^7)_4\text{Cl}_6(\text{CH}_3\text{OH})_8(\text{H}_2\text{O})_4]\cdot\text{Cl}_2\cdot(\text{CH}_3\text{OH})_9\cdot(\text{H}_2\text{O})_3$ (**24**, $\text{H}_3\text{L}^7 = 2\text{-}[2\text{-}(2\text{-hydroxy-3-methoxybenzylidene)-hydrazineyl}-2\text{-oxo-N-}(\text{pyridin-2-ylmethyl)} \text{acetamide}]$) 和 $[\text{Cu}_4\text{Tb}_4(\text{L}^7)_4\text{Cl}_6(\text{CH}_3\text{OH})_2(\text{H}_2\text{O})_{10}]\cdot\text{Cl}_2\cdot(\text{H}_2\text{O})_x$ (**25**)。这两个配合体表现出同构性。在化合物 **24** 中, 四个 Dy^{III} 离子几乎线性排列, 四个 Cu^{II} 离子分散在线性 $[\text{Dy}_4]$ 单元的两侧。最小不对称单元可被视为由蝶形 $[\text{Cu}_2\text{Dy}_2]$ 单元组成, 其中两个 Cu^{II} 离子形成“蝴蝶”的翅膀, 两个 Dy^{III} 离子构成“蝴蝶”体, 这两个 Dy^{III} 离子由两个 $(\text{L}^7)^{3-}$ 配体提供的两个 $\mu_2\text{-O}$ 原子桥接(图 13)。**24** 和 **25** 的直流磁化率测量表明, Cu^{II} 和 Ln^{III} 离子之间存在铁磁相互作用, Ln^{III} 具有强磁各向异性。此外, 由于 Ln-Ln 距离相对较短, Ln^{III} 离子之间的磁交换相互作用不容忽视。同时, 交流磁化率测量揭示了两种配合物在零场条件下的缓慢磁弛豫行为。具体而言, **24** 表现出 54 K 的有效能垒, 指前因子 τ_0 为 2.18×10^{-9} s。在配合物 **24** 中, Dy^{III} 离子表现为 Kramers 离子, 3d 金属与 Dy^{III} 之间的磁耦合有效抑制了 QTM。此外, Dy^{III} 基配合物在低对称配位环境中也表现出 SMM 行为。相反, 在化合物 **25** 中, Tb^{III} 是非 Kramers 离子, 存在于低对称配位环境中, 从而阻碍了慢磁弛豫行为的观察[30]。

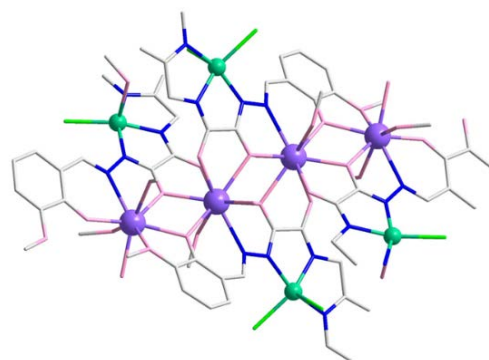


Figure 13. The molecular structure of **23**. Color code: Cu^{II} , green; Dy, purple; O, pink; N, blue; C, gray; Cl, bright green. H atoms are omitted for clarity. Reproduced from [30]

图 13. 配合物 **23** 的分子结构图。颜色: Cu^{II} , 绿色; Dy, 紫色; O、粉红色; N、蓝色; C、灰色; Cl, 亮绿色。为了清楚起见省略了 H 原子。经参考文献[30]转载

2013 年，童明良研究组利用两步原位反应合成了一个单分子磁体 $Dy^{III}Cu^{II}_7(OH)_2(L^8)_2(L^9)_2(OAc)_8(No_3)_2(H_2O)_4](No_3)_2 \cdot 8.5H_2O$ (**26**) (图 14(a))。在该配合物中，两个三角形[DyCu₂]单元共享一个 Dy^{III} 离子，并由配体 L⁸ 和 L⁹ 桥接，形成蝴蝶形[DyCu₄]单元。随后，八个 OAc⁻ 基团采用两种不同的配位模式，将两个[DyCu₄]单元连接起来，形成配合物 **26** (图 14(b))。直流磁化率测量表明，在低温下，配合物 **26** 表现出主要的铁磁相互作用和显著的磁各向异性。在零外部磁场中，在 **26** 的虚部交流磁化率中观察到明显的频率依赖性行为，表明存在具有有效能量势垒 $U_{eff} = 18.0 (3)$ K 的 SMM 行为[31]。

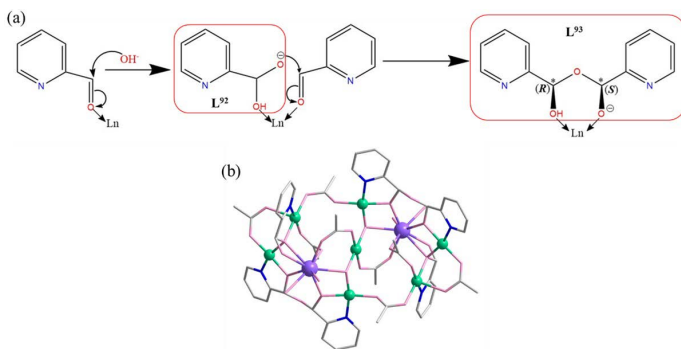


Figure 14. A two-step in situ reaction (a) and the molecular structure of **26** (b)
图 14. 两步原位反应(a)和 **26** 的分子结构(b)

2017 年，严振政领导的课题组合成了一系列空竹类非核团簇，表示为 $[LnCu_8(OH)_8(2-ma)_8(Cl)_2][ClO_4] \cdot xH_2O$ ($Ln = Tb$ (**27**), Ho (**28**), Dy (**29**), Er (**30**), Tm (**31**), Yb (**32**), 2-ma = 2-methylalanine)。所有七个化合物都表现出同构性。在它们的金属核内， Ln^{III} 离子被夹在两个 $Cu_4(OH)_4$ (8-MC-4) 单元之间。每个 8-MC-4 单元由一个八元交替的 Cu-O 环组成。此外， Cu^{II} 离子与 2-ma 配体的羧酸盐氧和氨基氮配位，而氯离子位于由四个 2-ma 配体和 Cu^{II} 离子形成的“碗”中(图 15(a))。在零外加直流场下的交流磁化率测试中，只有配合物 **30** 表现出缓慢的磁弛豫行为。随后，在施加小的直流场时，观察到 **29**、**31** 和 **32** 也显示出与频率相关的行为。值得注意的是，**30** 中虚部信号的频率依赖性更加明显。零直流场下的配合物 **30** 和直流场下配合物 **31** 在较低温度下都表现出量子磁化隧穿(QTM)。因此，通过与各种弛豫过程拟合，确定配合物 **29-32** 的能垒位于 23 K 至 33 K 的范围内(图 15(b))。理论计算表明，配合物 **29-32** 的能垒差异可以忽略不计，基本上与参数 $|J_{Cu-Cu}| = 20$ K 一致。尽管两个 $\{Cu_4\}$ 单元都是单线态基态，但可以推断这些化合物的慢磁弛豫行为受到 $Cu_4-Ln^{III}-Cu_4$ 相互作用的影响[32]。

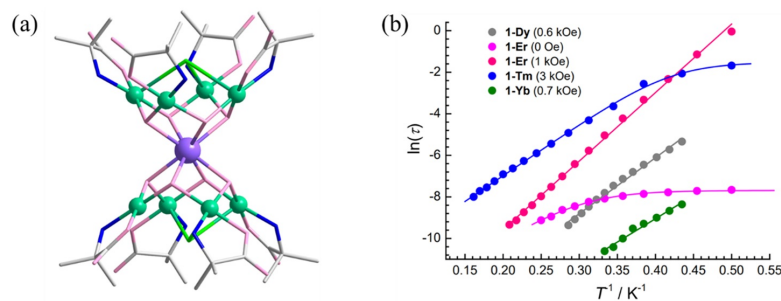


Figure 15. The molecular structure of **30** (a) and Arrhenius plot for complex **29-32** under corresponding dc field (b). Color code: Cu^{II} , green; Er, purple; O, pink; N, blue; C, gray; Cl, bright green. H atoms are omitted for clarity. The solid line corresponds to the fit of the data. Reproduced from [32]

图 15. **30** 的分子结构图(a)和配合物 **29-32** 在相应直流场下的 Arrhenius 图(b)。颜色： Cu^{II} ，绿色；Er，紫色；O、粉红色；N、蓝色；C、灰色；Cl，亮绿色。为了清楚起见省略了 H 原子。实线对应于数据的拟合。转载自[32]

2021年, 童明良研究团队在单层金属宏晶 $\text{Dy}[\text{15-MC}_{\text{Cu}^{\text{II}}}-5]$ (**33**) 的基础上, 合成了一种具有独特双层三明治结构的配合物, 记为 $\{\text{Dy}[\text{15-MC}_{\text{Cu}^{\text{II}}}-5]\}_2$ (**34**)。值得注意的是, 化合物 **33** 与化合物 **18** 具有同构性, 而化合物 **34** 包含两个由 OH^- 桥接的 $\text{Dy}[\text{15-MC}_{\text{Cu}^{\text{II}}}-5]$ 单元, 其中两个去质子化的水杨醛配体占据 $\text{Dy}[\text{15-MC}_{\text{Cu}^{\text{II}}}-5]$ 单元内的轴向位置。化合物 **34** 代表了仅由 OH^- 桥接的双层金属丙烯的第一个例子(图 16)。磁性分析表明, **33** 和 **34** 在 $\text{Cu}^{\text{II}}-\text{Cu}^{\text{II}}$ 之间都表现出反铁磁相互作用, 而 $\text{Dy}^{\text{III}}-\text{Cu}^{\text{II}}$ 和/或 $\text{Dy}^{\text{III}}-\text{Dy}^{\text{III}}$ 之间可能存在铁磁交换相互作用。**33** 和 **34** 都表现出缓慢的磁弛豫行为, 最高有效能垒分别达到 900(31) K 和 838(53) K, 显示出优异的 SMM 特性。此外, **33** 呈现蝶形磁滞回线。在沿轴向引入铁磁耦合后, 在较低温度下, **34** 的磁弛豫时间明显慢于 **33**, 磁滞回线的开启温度提高到 6 K。理论计算证实, 当 Dy^{III} 离子的局部磁各向异性轴几乎共线时, $\text{Dy}^{\text{III}}-\text{Dy}^{\text{III}}$ 的轴向铁磁耦合抑制了 QTM [33]。

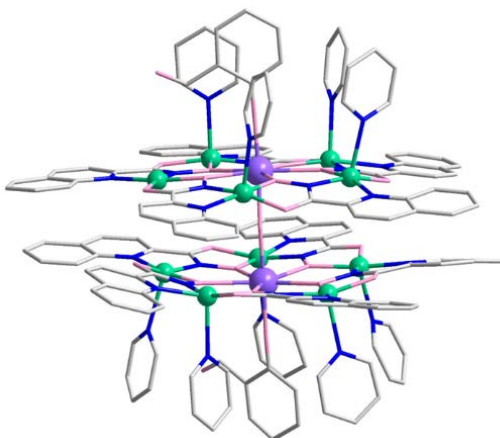


Figure 16. The molecular structure for **34**. Color code: Cu^{II} , green; Dy , purple; O, pink; N, blue; C, gray. H atoms are omitted for clarity. Reproduced from [33]

图 16. **34** 的分子结构图。颜色: Cu^{II} , 绿色; Dy , 紫色; O、粉红色; N、蓝色; C、灰色。为了清楚起见省略了 H 原子。转载自[33]

3. 结论

综合以上研究进展, 本文综述了不同结构类型, 包括从二核到多核的且磁学性能优异的 Cu-Ln 单分子磁体。二核结构表现出显著的磁性各向异性, 其结构简单易于合成, 是一个铜离子与一个稀土离子通过桥联配体连接而成的; 多核更为复杂, 选择不同配体和不同数量金属离子会形成不同的几何形态, 如线性, 环状, 四边形等等。稀土离子的选择也是极为重要的, Dy 和 Tb 离子具有强烈的自旋 - 轨道耦合和高的磁各向异性, 是制备高性能 SMM 的理想候选, 相比较而言 Gd 离子缺乏耦合, 其磁各向异性较弱, 因此磁学性能也较差, 因此本综述都是铜离子与镝或铽跟不同多齿配体的结合。

尽管在过去的几年里取得了显著的进展, 但仍有许多挑战需要克服, 例如致力于如何提高工作温度, 使其能在更宽的温度范围内表现出优异的磁性; 进一步设计合成新型配体, 来优化 Cu-Ln 单分子磁体的结构, 增强其稳定性和磁学性能; 同时开发多功能材料, 同时具备光电磁多重响应特性的复合材料也是在传感器和信息处理领域的新方向。

基金项目

江苏省研究生科研与实践创新计划项目(KYCX24_3546、SJCX24_1995、SJCX24_1992), 南通大学大型仪器开放基金资助(KFJN2471、KFJN2437)。

参考文献

- [1] Shukla, P., Das, S., Bag, P. and Dey, A. (2023) Magnetic Materials Based on Heterometallic Cr^{II/III}-Ln^{III} Complexes. *Inorganic Chemistry Frontiers*, **10**, 4322-4357. <https://doi.org/10.1039/d3qi00193h>
- [2] Winpenny, R.E.P. (2008) Quantum Information Processing Using Molecular Nanomagnets as Qubits. *Angewandte Chemie International Edition*, **47**, 7992-7994. <https://doi.org/10.1002/anie.200802742>
- [3] Leuenberger, M.N. and Loss, D. (2001) Quantum Computing in Molecular Magnets. *Nature*, **410**, 789-793. <https://doi.org/10.1038/35071024>
- [4] Salerno, E.V., Kampf, J.W., Pecoraro, V.L. and Mallah, T. (2021) Magnetic Properties of Two Gd^{III}fe^{III}₄ Metalla-crowns and Strategies for Optimizing the Magnetocaloric Effect of This Topology. *Inorganic Chemistry Frontiers*, **8**, 2611-2623. <https://doi.org/10.1039/d1qi00207d>
- [5] Wang, J., Sun, C., Zheng, Q., Wang, D., Chen, Y., Ju, J., et al. (2023) Lanthanide Single-Molecule Magnets: Synthetic Strategy, Structures, Properties and Recent Advances. *Chemistry—An Asian Journal*, **18**, e202201297. <https://doi.org/10.1002/asia.202201297>
- [6] Fan, J., Yu, H., Lin, Y., Qi, M., Kong, X., Sun, C., et al. (2024) An Organophosphate 3d-4f Heterometallic Polyoxoniobate Nanowire. *Nanoscale*, **16**, 12420-12423. <https://doi.org/10.1039/d4nr01619j>
- [7] Wang, H., Zhu, Z., Peng, J. and Zou, H. (2021) Heterometallic 3d/4f-Metal Complexes: Structure and Magnetism. *Journal of Cluster Science*, **33**, 1299-1325. <https://doi.org/10.1007/s10876-021-02084-7>
- [8] Bartholomew, A.K., Meirzadeh, E., Stone, I.B., Koay, C.S., Nuckolls, C., Steigerwald, M.L., et al. (2022) Superatom Regiochemistry Dictates the Assembly and Surface Reactivity of a Two-Dimensional Material. *Journal of the American Chemical Society*, **144**, 1119-1124. <https://doi.org/10.1021/jacs.1c12072>
- [9] Jin, P., Yu, K., Luo, Q., Liu, Y., Zhai, Y. and Zheng, Y. (2022) Tetraanionic arachno-Carboranyl Ligand Imparts Strong Axiality to Terbium(III) Single-Molecule Magnets. *Angewandte Chemie International Edition*, **61**, e202203285. <https://doi.org/10.1002/anie.202203285>
- [10] McClain, K.R., Kwon, H., Chakarawet, K., Nabi, R., Kragskow, J.G.C., Chilton, N.F., et al. (2023) A Trinuclear Gadolinium Cluster with a Three-Center One-Electron Bond and an S=11 Ground State. *Journal of the American Chemical Society*, **145**, 8996-9002. <https://doi.org/10.1021/jacs.3c00182>
- [11] Wang, J., Li, Q., Wu, S., Chen, Y., Wan, R., Huang, G., et al. (2021) Opening Magnetic Hysteresis by Axial Ferromagnetic Coupling: From Mono-Decker to Double-Decker Metalla-crown. *Angewandte Chemie International Edition*, **60**, 5299-5306. <https://doi.org/10.1002/anie.202014993>
- [12] Münzfeld, L., Gillhuber, S., Hauser, A., Lebedkin, S., Hädinger, P., Knöfel, N.D., et al. (2023) Synthesis and Properties of Cyclic Sandwich Compounds. *Nature*, **620**, 92-96. <https://doi.org/10.1038/s41586-023-06192-4>
- [13] Neumann, T., Thompson, B.C., Hebron, D., Graycon, D.M., Collauto, A., Roessler, M.M., et al. (2024) Heterobimetallic 3d-4f Complexes Supported by a Schiff-Base Tripodal Ligand. *Dalton Transactions*, **53**, 9921-9932. <https://doi.org/10.1039/d3dt03760f>
- [14] Wang, H., Zhang, K., Song, Y. and Pan, Z. (2021) Recent Advances in 3d-4f Magnetic Complexes with Several Types of Non-Carboxylate Organic Ligands. *Inorganica Chimica Acta*, **521**, Article 120318. <https://doi.org/10.1016/j.ica.2021.120318>
- [15] Peng, Y. and Powell, A.K. (2021) What Do 3d-4f Butterflies Tell Us? *Coordination Chemistry Reviews*, **426**, Article 213490. <https://doi.org/10.1016/j.ccr.2020.213490>
- [16] Oyarzabal, I., Echenique-Errandonea, E., San Sebastián, E., Rodríguez-Díéguez, A., Seco, J.M. and Colacio, E. (2021) Synthesis, Structural Features and Physical Properties of a Family of Triply Bridged Dinuclear 3d-4f Complexes. *Magnetochemistry*, **7**, Article 22. <https://doi.org/10.3390/magnetochemistry7020022>
- [17] Dey, A., Bag, P., Kalita, P. and Chandrasekhar, V. (2021) Heterometallic Cu^{II}-Ln^{III} Complexes: Single Molecule Magnets and Magnetic Refrigerants. *Coordination Chemistry Reviews*, **432**, Article 213707. <https://doi.org/10.1016/j.ccr.2020.213707>
- [18] Vincent, A.H., Whyatt, Y.L., Chilton, N.F. and Long, J.R. (2023) Strong Axiality in a Dysprosium(III) Bis(Borolide) Complex Leads to Magnetic Blocking at 65 K. *Journal of the American Chemical Society*, **145**, 1572-1579. <https://doi.org/10.1021/jacs.2c08568>
- [19] Wang, Y., Luo, Q. and Zheng, Y. (2024) Organolanthanide Single-Molecule Magnets with Heterocyclic Ligands. *Angewandte Chemie International Edition*, e202407016. <https://doi.org/10.1002/anie.202407016>
- [20] Kajiwara, T., Takahashi, K., Hiraizumi, T., Takaishi, S. and Yamashita, M. (2009) Coordination Enhancement of Single-Molecule Magnet Behavior of Tb(III)-Cu(II) Dinuclear Systems. *Polyhedron*, **28**, 1860-1863. <https://doi.org/10.1016/j.poly.2009.02.010>
- [21] Ishida, T., Watanabe, R., Fujiwara, K., Okazawa, A., Kojima, N., Tanaka, G., et al. (2012) Exchange Coupling in

- TbCu and DyCu Single-Molecule Magnets and Related Lanthanide and Vanadium Analogs. *Dalton Transactions*, **41**, 13609-13619. <https://doi.org/10.1039/c2dt31169k>
- [22] Mori, F., Nyui, T., Ishida, T., Nogami, T., Choi, K. and Nojiri, H. (2006) Oximate-Bridged Trinuclear Dy-Cu-Dy Complex Behaving as a Single-Molecule Magnet and Its Mechanistic Investigation. *Journal of the American Chemical Society*, **128**, 1440-1441. <https://doi.org/10.1021/ja057183f>
- [23] Chen, J., Yan, H., Wang, T. and Sun, W. (2024) Heteronuclear Complexes [MDyM](M=Cu; Zn; Ni) Constructed by Schiff Base Ligands with Different Amine Backbone Exhibiting Significant Single-Molecule Magnets. *Journal of Molecular Structure*, **1311**, Article 138473. <https://doi.org/10.1016/j.molstruc.2024.138473>
- [24] Osa, S., Kido, T., Matsumoto, N., Re, N., Pochaba, A. and Mrozniski, J. (2003) A Tetranuclear 3d-4f Single Molecule Magnet: $[\text{Cu}^{\text{II}}\text{LTb}^{\text{III}}(\text{hfac})_2]_2$. *Journal of the American Chemical Society*, **126**, 420-421. <https://doi.org/10.1021/ja037365e>
- [25] Huang, X., Zhou, C., Wei, H. and Wang, X. (2013) End-on Azido-Bridged 3d-4f Complexes Showing Single-Molecule-Magnet Property. *Inorganic Chemistry*, **52**, 7314-7316. <https://doi.org/10.1021/ic400986y>
- [26] Heras Ojea, M.J., Milway, V.A., Velmurugan, G., Thomas, L.H., Coles, S.J., Wilson, C., et al. (2016) Enhancement of $\text{Tb}^{\text{III}}\text{-Cu}^{\text{II}}$ Single-Molecule Magnet Performance through Structural Modification. *Chemistry—A European Journal*, **22**, 12839-12848. <https://doi.org/10.1002/chem.201601971>
- [27] Alexandropoulos, D.I., Cunha-Silva, L., Tang, J. and Stamatatos, T.C. (2018) Heterometallic Cu/Ln Cluster Chemistry: Ferromagnetically-Coupled $\{\text{Cu}_4\text{Ln}_2\}$ Complexes Exhibiting Single-Molecule Magnetism and Magnetocaloric Properties. *Dalton Transactions*, **47**, 11934-11941. <https://doi.org/10.1039/c8dt01780h>
- [28] Wang, J., Ruan, Z., Li, Q., Chen, Y., Huang, G., Liu, J., et al. (2019) Slow Magnetic Relaxation in a $\{\text{EuCu}_5\}$ Metalla-crown. *Dalton Transactions*, **48**, 1686-1692. <https://doi.org/10.1039/c8dt04814b>
- [29] Dey, A., Das, S., Kundu, S., Mondal, A., Rouzières, M., Mathonière, C., et al. (2017) Heterometallic Heptanuclear $[\text{Cu}_5\text{Ln}_2]$ ($\text{Ln}=\text{Tb}$, Dy, and Ho) Single-Molecule Magnets Organized in One-Dimensional Coordination Polymeric Network. *Inorganic Chemistry*, **56**, 14612-14623. <https://doi.org/10.1021/acs.inorgchem.7b02450>
- [30] Zhao, X., Li, G., Ma, J. and Liu, W. (2020) Two Octanuclear $\{\text{Cu}_4\text{Ln}_4\}$ ($\text{Ln}=\text{Dy}$ or Tb) Complexes with a Butterfly-Shaped Unit Exhibiting Zero-Field Single-Molecule Magnet Behavior. *Inorganic Chemistry*, **59**, 2328-2336. <https://doi.org/10.1021/acs.inorgchem.9b03137>
- [31] Liu, J., Chen, Y., Li, Q., Gómez-Coca, S., Aravena, D., Ruiz, E., et al. (2013) Two 3d-4f Nanomagnets Formed via a Two-Step In Situ Reaction of Picolinaldehyde. *Chemical Communications*, **49**, 6549-6551. <https://doi.org/10.1039/c3cc43200a>
- [32] Zhou, G., Han, T., Ding, Y., Chilton, N.F. and Zheng, Y. (2017) Metallacrowns as Templates for Diabolo-Like $\{\text{LnCu}_8\}$ Complexes with Nearly Perfect Square Antiprismatic Geometry. *Chemistry—A European Journal*, **23**, 15617-15622. <https://doi.org/10.1002/chem.201703830>
- [33] Wang, J., Li, Q., Wu, S., Chen, Y., Wan, R., Huang, G., et al. (2021) Opening Magnetic Hysteresis by Axial Ferromagnetic Coupling: From Mono-Decker to Double-Decker Metallacrown. *Angewandte Chemie International Edition*, **60**, 5299-5306. <https://doi.org/10.1002/anie.202014993>
- [34] Aronica, C., Pilet, G., Chastanet, G., Wernsdorfer, W., Jacquot, J. and Luneau, D. (2006) A Nonanuclear Dysprosium(III)-Copper(II) Complex Exhibiting Single-Molecule Magnet Behavior with Very Slow Zero-Field Relaxation. *Angewandte Chemie International Edition*, **45**, 4659-4662. <https://doi.org/10.1002/anie.200600513>
- [35] Costes, J., Dahan, F. and Wernsdorfer, W. (2005) Heterodinuclear Cu-Tb Single-Molecule Magnet. *Inorganic Chemistry*, **45**, 5-7. <https://doi.org/10.1021/ic050563h>
- [36] Han, Y. and Huynh, H.V. (2011) Pyrazolin-4-Ylidenes: A New Class of Intriguing Ligands. *Dalton Transactions*, **40**, 2141-2147. <https://doi.org/10.1039/c0dt01037e>
- [37] Kajiwara, T., Nakano, M., Takahashi, K., Takaishi, S. and Yamashita, M. (2010) Structural Design of Easy-Axis Magnetic Anisotropy and Determination of Anisotropic Parameters of $\text{Ln}^{\text{III}}\text{-Cu}^{\text{II}}$ Single-Molecule Magnets. *Chemistry—A European Journal*, **17**, 196-205. <https://doi.org/10.1002/chem.201002434>
- [38] Langley, S.K., Ungur, L., Chilton, N.F., Moubaraki, B., Chibotaru, L.F. and Murray, K.S. (2011) Structure, Magnetism and Theory of a Family of Nonanuclear $\text{Cu}^{\text{II}}_5\text{Ln}^{\text{III}}_4$ -Triethanolamine Clusters Displaying Single-Molecule Magnet Behaviour. *Chemistry—A European Journal*, **17**, 9209-9218. <https://doi.org/10.1002/chem.201100218>
- [39] Chandrasekhar, V., Dey, A., Das, S., Rouzières, M. and Clérac, R. (2013) Syntheses, Structures, and Magnetic Properties of a Family of Heterometallic Heptanuclear $[\text{Cu}_5\text{Ln}_2]$ ($\text{Ln}=\text{Y(III)}$, Lu(III) , Dy(III) , Ho(III) , Er(III) , and Yb(III)) Complexes: Observation of SMM Behavior for the Dy(III) and Ho(III) Analogues. *Inorganic Chemistry*, **52**, 2588-2598. <https://doi.org/10.1021/ic302614k>
- [40] Feltham, H.L.C., Clérac, R., Ungur, L., Chibotaru, L.F., Powell, A.K. and Brooker, S. (2013) By Design: A Macroyclic 3d-4f Single-Molecule Magnet with Quantifiable Zero-Field Slow Relaxation of Magnetization. *Inorganic Chemistry*,

- istry*, **52**, 3236-3240. <https://doi.org/10.1021/ic302735j>
- [41] Liu, J., Lin, W., Chen, Y., Gómez-Coca, S., Aravena, D., Ruiz, E., et al. (2013) Cu^{II}-Gd^{III} Cryogenic Magnetic Refrigerants and Cu₈Dy₉ Single-Molecule Magnet Generated by in Situ Reactions of Picolinaldehyde and Acetylpyridine: Experimental and Theoretical Study. *Chemistry—A European Journal*, **19**, 17567-17577. <https://doi.org/10.1002/chem.201303275>
- [42] Escobar, L.B.L., Guedes, G.P., Soriano, S., Speziali, N.L., Jordão, A.K., Cunha, A.C., et al. (2014) New Families of Hetero-Tri-Spin 2p-3d-4f Complexes: Synthesis, Crystal Structures, and Magnetic Properties. *Inorganic Chemistry*, **53**, 7508-7517. <https://doi.org/10.1021/ic5008044>
- [43] Ghosh, S., Ida, Y., Ishida, T. and Ghosh, A. (2014) Linker Stoichiometry-Controlled Stepwise Supramolecular Growth of a Flexible Cu₂Tb Single Molecule Magnet from Monomer to Dimer to One-Dimensional Chain. *Crystal Growth & Design*, **14**, 2588-2598. <https://doi.org/10.1021/cg500290m>
- [44] Hu, K., Wu, S., Cui, A. and Kou, H. (2014) Synthesis, Structure, and Magnetic Properties of Heterotrimetallic Tetranuclear Complexes. *Transition Metal Chemistry*, **39**, 713-718. <https://doi.org/10.1007/s11243-014-9854-5>
- [45] Kettles, F.J., Milway, V.A., Tuna, F., Valiente, R., Thomas, L.H., Wernsdorfer, W., et al. (2014) Exchange Interactions at the Origin of Slow Relaxation of the Magnetization in {TbCu₃} and {DyCu₃} Single-Molecule Magnets. *Inorganic Chemistry*, **53**, 8970-8978. <https://doi.org/10.1021/ic500885r>
- [46] Xue, S., Guo, Y., Zhao, L., Zhang, H. and Tang, J. (2014) Molecular Magnetic Investigation of a Family of Octanuclear [Cu₆Ln₂] Nanoclusters. *Inorganic Chemistry*, **53**, 8165-8171. <https://doi.org/10.1021/ic501226y>
- [47] Dermitzaki, D., Raptopoulou, C.P., Psycharis, V., Escuer, A., Perlepes, S.P. and Stamatatos, T.C. (2015) Nonemployed Simple Carboxylate Ions in Well-Investigated Areas of Heterometallic Carboxylate Cluster Chemistry: A New Family of {Cu^{II}₄Ln^{III}₈} Complexes Bearing *tert*-Butylacetate Bridging Ligands. *Inorganic Chemistry*, **54**, 7555-7561. <https://doi.org/10.1021/acs.inorgchem.5b01179>
- [48] Wang, X., Hu, P., Li, Y. and Li, L. (2014) Construction of Nitronyl Nitroxide-Based 3d-4f Clusters: Structure and Magnetism. *Chemistry—A European Journal*, **10**, 325-328. <https://doi.org/10.1002/asia.201403165>
- [49] Wu, J., Zhao, L., Guo, M. and Tang, J. (2015) Constructing Supramolecular Grids: From 4f Square to 3d-4f Grid. *Chemical Communications*, **51**, 17317-17320. <https://doi.org/10.1039/c5cc06960b>
- [50] Dhers, S., Feltham, H.L.C., Rouzières, M., Clérac, R. and Brooker, S. (2016) Macroyclic {3d-4f} SMMs as Building Blocks for 1D-Polymers: Selective Bridging of 4f Ions by Use of an O-Donor Ligand. *Dalton Transactions*, **45**, 18089-18093. <https://doi.org/10.1039/c6dt03734h>
- [51] Gupta, T., Beg, M.F. and Rajaraman, G. (2016) Role of Single-Ion Anisotropy and Magnetic Exchange Interactions in Suppressing Zero-Field Tunnelling in {3d-4f} Single Molecule Magnets. *Inorganic Chemistry*, **55**, 11201-11215. <https://doi.org/10.1021/acs.inorgchem.6b01831>
- [52] Wu, J., Zhao, L., Zhang, L., Li, X., Guo, M., Powell, A.K., et al. (2016) Macroscopic Hexagonal Tubes of 3d-4f Metallocycles. *Angewandte Chemie International Edition*, **55**, 15574-15578. <https://doi.org/10.1002/anie.201609539>
- [53] Wu, J., Zhao, L., Zhang, L., Li, X., Guo, M. and Tang, J. (2016) Metallosupramolecular Coordination Complexes: The Design of Heterometallic 3d-4f Gridlike Structures. *Inorganic Chemistry*, **55**, 5514-5519. <https://doi.org/10.1021/acs.inorgchem.6b00529>
- [54] Alexandropoulos, D.I., Poole, K.M., Cunha-Silva, L., Ahmad Sheikh, J., Wernsdorfer, W., Christou, G., et al. (2017) A Family of ‘Windmill’-Like {Cu₆Ln₁₂} Complexes Exhibiting Single-Molecule Magnetism Behavior and Large Magnetic Entropy Changes. *Chemical Communications*, **53**, 4266-4269. <https://doi.org/10.1039/c7cc01382e>
- [55] Biswas, S., Bag, P., Das, S., Kundu, S., van Leusen, J., Kögerler, P., et al. (2017) Heterometallic [Cu₂Ln₃] (Ln=Dy^{III}, Gd^{III} and Ho^{III}) and [Cu₄Ln₂] (Ln=Dy^{III} and Ho^{III}) Compounds: Synthesis, Structure, and Magnetism. *European Journal of Inorganic Chemistry*, **2017**, 1129-1142. <https://doi.org/10.1002/ejic.201601210>
- [56] Kühne, I.A., Griffiths, K., Hutchings, A., Townrow, O.P.E., Eichhöfer, A., Anson, C.E., et al. (2017) Stepwise Investigation of the Influences of Steric Groups versus Counterions to Target Cu/Dy Complexes. *Crystal Growth & Design*, **17**, 5178-5190. <https://doi.org/10.1021/acs.cgd.7b00648>
- [57] Li, C., Li, H., Xie, J., Yang, M., Wang, X. and Li, L. (2017) {[Ln(hfac)₃]₂[Cu(hfac)₂]₃(NIT-Pyrim)₂(H₂O)₂} (Ln^{III}=Gd, Ho, Er): Unique Nitronyl Nitroxide Bridged 3d-4f Heterometallic Clusters. *European Journal of Inorganic Chemistry*, **2018**, 525-530. <https://doi.org/10.1002/ejic.201700576>
- [58] Ueno, T., Fujinami, T., Matsumoto, N., Furusawa, M., Irie, R., Re, N., et al. (2017) Circular and Chainlike Copper(II)-Lanthanide(III) Complexes Generated by Assembly Reactions of Racemic and Chiral Copper(II) Cross-Linking Ligand Complexes with Ln^{III}(No₃)₃·6H₂O (Ln^{III}=Gd^{III}, Tb^{III}, Dy^{III}). *Inorganic Chemistry*, **56**, 1679-1695. <https://doi.org/10.1021/acs.inorgchem.6b02668>
- [59] Yang, M., Xie, J., Sun, Z., Li, L. and Sutter, J. (2017) Slow Magnetic Relaxation in Ladder-Type and Single-Strand 2p-3d-4f Heterotrinspin Chains. *Inorganic Chemistry*, **56**, 13482-13490. <https://doi.org/10.1021/acs.inorgchem.7b02204>

- [60] Dermitzaki, D., Bistola, O., Pissas, M., Pscharis, V., Sanakis, Y. and Raptopoulou, C.P. (2018) Heptanuclear Heterometallic Cu²⁺Ln₂ (Ln=Gd, Tb) Complexes: Synthesis, Crystal Structures, and Magnetic Properties Studies. *Polyhedron*, **150**, 47-53. <https://doi.org/10.1016/j.poly.2018.05.003>
- [61] Dey, A., Das, S., Palacios, M.A., Colacio, E. and Chandrasekhar, V. (2018) Single-Molecule Magnet and Magneto-thermal Properties of Two-Dimensional Polymers Containing Heterometallic [Cu₅Ln₂] (Ln=Gd^{III} and Dy^{III}) Motifs. *European Journal of Inorganic Chemistry*, **2018**, 1645-1654. <https://doi.org/10.1002/ejic.201701429>
- [62] Dey, B., Roy, S., Mondal, A.K., Santra, A. and Konar, S. (2018) Zero Field SMM Behavior and Magnetic Refrigeration in Rare Heterometallic Double Stranded Helicates of Cu₂Ln₂ (Ln=Dy, Tb, Gd). *European Journal of Inorganic Chemistry*, **2018**, 2429-2436. <https://doi.org/10.1002/ejic.201800075>
- [63] Li, H., Sun, Z., Sun, J., Xi, L., Guo, J., Sun, G., et al. (2018) Single-Molecule Magnet Behavior in a Cu²⁺-Decorated {Dy^{III}₂} Complex with Nitronyl Nitroxide Biradicals. *Journal of Materials Chemistry C*, **6**, 2060-2068. <https://doi.org/10.1039/c7tc05377k>
- [64] Worrell, A., Sun, D., Mayans, J., Lampropoulos, C., Escuer, A. and Stamatatos, T.C. (2018) Oximate-Based Ligands in 3d/4f-Metal Cluster Chemistry: A Family of {Cu₃Ln} Complexes with a “Propeller”-Like Topology and Single-Molecule Magnetic Behavior. *Inorganic Chemistry*, **57**, 13944-13952. <https://doi.org/10.1021/acs.inorgchem.8b02495>
- [65] Wu, J., Guo, M., Li, X., Zhao, L., Sun, Q., Layfield, R.A., et al. (2018) From Double-Shelled Grids to Supramolecular Frameworks. *Chemical Communications*, **54**, 12097-12100. <https://doi.org/10.1039/c8cc06411c>
- [66] Wu, J., Li, X., Guo, M., Zhao, L., Zhang, Y. and Tang, J. (2018) Realization of Toroidal Magnetic Moments in Heterometallic 3d-4f Metallocycles. *Chemical Communications*, **54**, 1065-1068. <https://doi.org/10.1039/c7cc09391h>
- [67] Chen, Y., Long, Q., Hu, Z., Wang, H., Huang, Z., Chen, W., et al. (2019) Synthesis, Crystal Structures and Magnetic Properties of a Series of Pentanuclear Heterometallic [Cu²⁺₃Ln^{III}₂] (Ln=Ho, Dy, and Gd) Complexes Containing Mixed Organic Ligands. *New Journal of Chemistry*, **43**, 8101-8108. <https://doi.org/10.1039/c9nj00892f>
- [68] Dermitzaki, D., Pscharis, V., Sanakis, Y., Stamatatos, T.C., Pissas, M. and Raptopoulou, C.P. (2019) Extending the Family of Heptanuclear Heterometallic Cu₅Ln₂ (Ln=Gd, Tb, Dy) Complexes: Synthesis, Crystal Structures, Magnetic and Magnetocaloric Studies. *Polyhedron*, **169**, 135-143. <https://doi.org/10.1016/j.poly.2019.05.004>
- [69] Mahapatra, P., Koizumi, N., Kanetomo, T., Ishida, T. and Ghosh, A. (2019) A Series of Cu²⁺-Ln^{III} Complexes of an N₂O₃ Donor Asymmetric Ligand and a Possible Cu²⁺-Tb^{III} SMM Candidate in No Bias Field. *New Journal of Chemistry*, **43**, 634-643. <https://doi.org/10.1039/c8nj03512a>
- [70] Maity, S., Mondal, A., Konar, S. and Ghosh, A. (2019) The Role of 3d-4f Exchange Interaction in SMM Behaviour and Magnetic Refrigeration of Carbonato Bridged Cu²⁺₂Ln^{III}₂ (Ln=Dy, Tb and Gd) Complexes of an Unsymmetrical N₂O₄ Donor Ligand. *Dalton Transactions*, **48**, 15170-15183. <https://doi.org/10.1039/c9dt02627d>
- [71] Shi, J.Y., Chen, P.Y., Wu, M.Z., Tian, L. and Liu, Z.Y. (2019) Synthesis of a Series of Hetero-Multi-Spin Ln₂Cu₃ Complexes Based on a Methyl-Pyrazole Nitronyl Nitroxide Radical with Slow Magnetic Relaxation Behaviors. *Dalton Transactions*, **48**, 9187-9193. <https://doi.org/10.1039/c9dt00981g>
- [72] Wang, K., Sun, J., Xi, L., Lu, J., Jing, P. and Li, L. (2019) Heterometallic Ln-Cu Complexes Derived from a Phenyl Pyrimidyl Substituted Nitronyl Nitroxide Biradical. *Dalton Transactions*, **48**, 14383-14389. <https://doi.org/10.1039/c9dt03081f>
- [73] Zhang, H., Yang, H., Yang, J., Li, D. and Dou, J. (2019) Single Molecular Magnet Behavior for a Copper(II)-Terbium(III) 15-Metallacrown-5 Complex Based on Pyrazinehydroxamic Acid. *Inorganica Chimica Acta*, **495**, Article 119014. <https://doi.org/10.1016/j.ica.2019.119014>
- [74] Chang, W., Yang, H., Tian, H., Li, D. and Dou, J. (2020) 3d-4f Metallacrown Complexes with a New Sandwich Core: Synthesis, Structures and Single Molecule Magnet Behavior. *New Journal of Chemistry*, **44**, 14145-14150. <https://doi.org/10.1039/d0nj00292e>
- [75] Maity, S., Bhunia, P., Ichihashi, K., Ishida, T. and Ghosh, A. (2020) SMM Behaviour of Heterometallic Dinuclear Cu²⁺Ln^{III} (Ln=Tb and Dy) Complexes Derived from N₂O₃ Donor Unsymmetrical Ligands. *New Journal of Chemistry*, **44**, 6197-6205. <https://doi.org/10.1039/d0nj00193g>
- [76] Yang, M., Liang, X., Zhang, Y., Ouyang, Z. and Dong, W. (2020) A Family of 3d-4f Cu-Ln Ladder-Like Complexes: Synthesis, Structures and Magnetic Properties. *Polyhedron*, **180**, Article 114435. <https://doi.org/10.1016/j.poly.2020.114435>
- [77] Ghosh, T.K., Maity, S., Mayans, J. and Ghosh, A. (2020) Family of Isomeric Cu²⁺-Ln^{III} (Ln=Gd, Tb, and Dy) Complexes Presenting Field-Induced Slow Relaxation of Magnetization Only for the Members Containing Gd^{III}. *Inorganic Chemistry*, **60**, 438-448. <https://doi.org/10.1021/acs.inorgchem.0c03129>
- [78] Li, H., Jing, P., Lu, J., Xi, L., Wang, Q., Ding, L., et al. (2021) Multifunctional Properties of {Cu²⁺₂Ln^{III}₂} Systems Involving Nitrogen-Rich Nitronyl Nitroxide: Single-Molecule Magnet Behavior, Luminescence, Magnetocaloric Effects

- and Heat Capacity. *Dalton Transactions*, **50**, 2854-2863. <https://doi.org/10.1039/d0dt04344c>
- [79] Zhang, S., Fan, X., Du, R., Shen, B., Song, X., Wei, X., et al. (2021) Synthesis, Crystal Structures and Magnetism of Cu^{II}Ln^{III} N₂O₄-Donor Coordination Compounds Involving Dicyanamides. *Polyhedron*, **206**, Article 115336. <https://doi.org/10.1016/j.poly.2021.115336>
- [80] Zhang, Y., Liang, X., Ouyang, Z. and Yang, M. (2021) Two 2p-3d-4f Complexes Constructed from Functionalized Nitronyl Nitroxides: Synthesis, Structure and Magnetic Properties. *Journal of Molecular Structure*, **1225**, Article 129155. <https://doi.org/10.1016/j.molstruc.2020.129155>
- [81] Dais, T.N., Takano, R., Yamaguchi, Y., Ishida, T. and Plieger, P.G. (2022) Metallocyclic Cu^{II}-Ln^{III} Single-Molecule Magnets from the Self-Assembly of 1,4-Diformylnaphthalene-2,3-Diol. *ACS Omega*, **7**, 5537-5546. <https://doi.org/10.1021/acsomega.1c07001>
- [82] Liu, C., Zhu, S., Lu, Y., Hao, X. and Wen, H. (2023) Homochiral Cu₆Dy₃ Single-Molecule Magnets Displaying Proton Conduction and a Strong Magneto-Optical Faraday Effect. *Inorganic Chemistry Frontiers*, **10**, 3714-3722. <https://doi.org/10.1039/d3qi00634d>